NASA TECHNICAL NOTE

NASA TN D-6685

NASA TN D-6685

MAGNETIC DIPOLE MOMENT DETERMINATION BY NEAR-FIELD ANALYSIS

by W. L. Eichhorn

Goddard Space Flight Center
Greenbelt, Md. 20771

NATIONAL AERONAUTICS AND SPACE ADMINISTRATION • WASHINGTON, D. C. • JULY 1972

1. Report No.	2. Government Accession No.	3. Recipient's Catalog No.
NASA TN D-6685		

4. Title and Subtitle	5. Report Date
Magnetic Dipole Moment Determination by Near-Field Analysis	July 1972
	6. Performing Organization Code
7. Author(s)	8. Performing Organization Report No.
W. L. Eichhorn	G-1034
9. Performing Organization Name and Address	10. Work Unit No.
Goddard Space Flight Center Greenbelt, Maryland 20771	11. Contract or Grant No.
	13. Type of Report and Period Covered
12. Sponsoring Agency Name and Address	Technical Note
National Aeronautics and Space Administration Washington, D.C. 20546	14. Sponsoring Agency Code

15. Supplementary Notes

16. Abstract

This report presents a method for determining the magnetic moment of a spacecraft from magnetic field data taken in a limited region of space close to the spacecraft. The spacecraft's magnetic field equations are derived from first principles. With measurements of this field restricted to certain points in space, the near-field equations for the spacecraft are derived. These equations are solved for the dipole moment by a least squares procedure. A method by which one can estimate the magnitude of the error in the calculations is also presented.

This technique was thoroughly tested on a computer. The test program is described and evaluated, and partial results are presented.

17. Key Words Suggested by Author	18. Distribution Statement
Magnetic dipole moment Magnetic field Vector spherical harmonics Spacecraft Near field Multipole	Unclassified—Unlimited

19. Security Classif. (of this report)	20. Security Classif. (of this page)	21. No. of Pages	22. Price
Unclassified	Unclassified	87	$3.00

* For sale by the National Technical Information Service, Springfield, Virginia 22151

CONTENTS

LIST OF SYMBOLS

a, b, A, B, C, D	Arbitrary constants.
$\mathbf{A}(\mathbf{r})$	Magnetic vector potential at the point $\mathbf{r}$.
$\mathbf{A}_{jm}(\mathbf{r})$	Pure multipole vector potential at the point $\mathbf{r}$.
a_{jm}, b_{jm}	General multipole moment coefficients.
$a_{jm}(\mathbf{k}), b_{jm}(\mathbf{k})$	Multipole moment coefficients produced by a point dipole at the point $\mathbf{k}$.
a_j	The multipole coefficient $a_{2j-1,1}$ divided by r_1^{2j+1}.
$A_m, A_0, A_m(A)$, $A_m(i, j, \cos\theta)$	Various Fourier coefficients.
$\mathbf{B}(\mathbf{r})$	Magnetic flux density at the point $\mathbf{r}$.
$\mathbf{B}_{jm}(\mathbf{r})$	Pure multipole magnetic flux density at the point $\mathbf{r}$.
$B_i(r, \phi, \cos\theta)$	Component of the magnetic field at the point $\mathbf{r} = (r, \theta, \phi)$.
B_{jpp}	Maximum field excursion seen on the jth sensor of the most distant probe.
B_{ip}	Maximum field seen on the jth sensor of the most distant probe.
B_e	Magnetization estimation of the source.
$\mathbf{B}_1$	Lowest order term in the expansion of $\mathbf{B}(\mathbf{r})$.
$C_{js}(J, M; m, q)$	Clebsch-Gordan coefficient.
$c_{ij}, c_{ij}(s)$	Near-field matrix elements.
C_i	The theoretical expression for y_i.
$dV, d^3\mathbf{r}, d^3\mathbf{k}, r^2\, dr\, d\Omega$	Infinitesimal volume elements.
$d\mathbf{N}_j, d\mathbf{N}_m$	Elements of torque.
$d\mathbf{S}$	Element of surface area.
$d\Omega$	Element of solid angle.

$d_i(j,m,r)$, $d_i'(j,m,r)$	Coefficients of the vector spherical harmonic $\mathbf{Y}^m_{j,j+1}(\theta,\phi)$.
D_{jm}	Amplitude of the vector spherical harmonic $\mathbf{Y}^m_{jk}(\theta,\phi)$.
D_k	Element of the data matrix D.
$\mathbf{e}_{+1}$, $\mathbf{e}_0$, $\mathbf{e}_{-1}$	Spherical unit vectors.
$e_j(s)$	Error in the least squares estimate of the jth multipole coefficient for the sth axis.
$e_{rj}(s)$	Element of the error matrix for the sth axis.
$E_{ij}(s,k)$	Single-dipole error function.
$F(h,z)$	Generating function for the Legendre polynomials.
$f(y)$, $f(y,z)$	Probability functions for the variables y, and y and z.
f, f', g	Arbitrary functions of r.
G	Measurement matrix.
G_{ij}	Measurement matrix element.
$g(r,r')$, $g_j(r,r')$	Green's functions.
G^m_{Jjq}	Eigenfunctions of the operation $\mathbf{J} = \mathbf{J}_1 + \mathbf{J}_2$.
$\mathbf{h}_j(s,\mathbf{k})$	Field function for the multipole coefficient $n_j(s,\mathbf{k})$.
$\mathbf{H}(\mathbf{r})$	Magnetic field intensity at the point $\mathbf{r}$.
I, I_{+1}, I_0, I_{-1}	Arbitrary integrals.
$\mathbf{J}(\mathbf{r})$	Current density at the point $\mathbf{r}$.
$\mathbf{J}$	Total angular moment in operator.
$K(j,m,r)$	Source term in the equation for $d_0(j,m,r)$.
$\mathbf{k}, \mathbf{r}, \mathbf{r}'$	Position vectors.
k	Magnitude of $\mathbf{k}$.
$\mathbf{L}$	Angular momentum operator $(-i\mathbf{r}\times\nabla)$.
$\mathbf{M}(\mathbf{r})$	Magnetization density at the point $\mathbf{r}$.
$\mathbf{m}$	Dipole moment.

$\mathbf{m}(\mathbf{k})$	Moment of a dipole at the point $\mathbf{k}$.
$M(s)$	Number of unknown multipole coefficients on the sth axis equations.
$\mathbf{N}$	Magnetic torque.
$n_j, n_j(s)$	Actual sth axis multipole coefficients of a source.
$n_j(s, \mathbf{k})$	Actual sth axis multipole coefficients for a dipole at the point $\mathbf{k}$.
$N(s)$	Number of Fourier coefficients involving the sth axis multipole moments.
N_p	Number of probes.
P	Arbitrary point in space.
$P_i^m(\cos\theta)$	Associated Legendre functions.
$q_r, q_r(s)$	Least squares estimate of the rth multipole coefficient n_r.
$q_r(s, \mathbf{k})$	Least squares estimate of $n_r(s, \mathbf{k})$.
$\mathbf{Q}_r(s, \mathbf{k})$	Percent error vector for $q_r(s, \mathbf{k})$.
$Q_r^M(s, \mathbf{k})$	Maximum value of the function $\mathbf{Q}_r(s, \mathbf{k})$.
$Q^S(\mathbf{k})$	An estimate of $Q_r^M(s, \mathbf{k})$.
Q_{jm}	Arbitrary function of Y_{jm} and Y_{jm}^*.
$q(y)$	Arbitrary function of y.
r, θ, ϕ	Spherical polar components of $\mathbf{r}$.
$\mathbf{r}, \boldsymbol{\theta}, \boldsymbol{\phi}$	Spherical polar unit vectors.
$r_>$	The greater of r, r'.
$r_<$	The lesser of r, r'.
r_i	Radius of the ith probe.
r_f	Radius of the farthest sensor.
r_{ij}	Ratio of r_i to r_j.
S	Magnetometer scale factor.
$S^2(y)$	Estimated standard deviation of the quantity y.
$S_{ij}(\mathbf{k})$	Zenith angle functions for the multipole coefficient $n_j(s, \mathbf{k})$.

$\mathbf{S}$	Spin operator.
s_p	Size parameter.
t, t_a	Variable in Student's distribution.
$U(\mathbf{r})$	Magnetic scalar potential.
$\mathbf{u}_1, \mathbf{u}_2, \mathbf{u}_3$	Cartesian unit vectors.
$\mathbf{V}$	Arbitrary vector.
V_{+1}, V_0, V_{-1}	Spherical components of $\mathbf{V}$.
V_1, V_2, V_3	Cartesian components of $\mathbf{V}$.
v_i	ith residual.
$w_i, w_i(s)$	Weighting functions for the ith near-field equation for the sth axis.
x_1, x_2, x_3	Cartesian components of $\mathbf{r}$.
X, X_i	Population means for the quantities x and x_i.
x	$\cos\theta$ [as in $P_j^m(x)$ only].
$Y_{jm}(\theta, \phi)$	Spherical harmonic.
$\mathbf{Y}_{jk}^m(\theta, \phi)$	Vector spherical harmonic.
y, z	Arbitrary quantities.
Y, Z	Population means of y and z.
$y_i, y_i(s)$	Average values of the ith Fourier coefficient for the sth axis.
$y_i(s, \mathbf{k})$	The ith Fourier coefficient for the sth axis produced by a dipole at the point $\mathbf{k}$.
$\bar{y}$	Average value of the quantity y.
$\Gamma(x)$	Gamma function of x.
δ_{ij}	Kronecker delta.
$\delta(\mathbf{r})$	Dirac delta function.
$\delta_i, \delta_i(s)$	The portion of the ith Fourier coefficient for the ith axis due to the multipole of order $M(s) + 1$ or higher.
δ	A known error limit.

ϵ	A small quantity.
ν	Number of degree of freedom $[N(s) - M(s)]$.
$\sigma^2(x)$, $\sigma_i^2(x)$	Variances of x.
ϕ_{jk}	Matrix element of the inverse matrix of G.
∇	Laplacian operator.
$\Delta(r)$	Differential operator.
$\psi_1, \psi_2, \psi_3, \omega$	Quantities in the equations for the components of the magnetic field **B** of an off-center dipole.

MAGNETIC DIPOLE MOMENT DETERMINATION BY NEAR-FIELD ANALYSIS

by
W. L. Eichhorn
Goddard Space Flight Center

CHAPTER I

INTRODUCTION

A spacecraft orbiting in the earth's magnetic field will be subject to forces and torques resulting from the interaction between the earth's field and onboard currents and magnetic matter. Since the earth's field is uniform over the volume of the spacecraft, this interaction may be described solely in terms of the dipole moment of the spacecraft. There are two ways to determine this moment. One is by direct measurement of the torque acting on the spacecraft in a known magnetic field. The other is by a suitable analysis of the spacecraft magnetic field. In cases where torque measurement is impossible, one must rely entirely on magnetic measurements.

This report presents a refined version of the method of dipole moment determination described in Reference 1. It discusses a technique designed to analyze the near-field portion of the spacecraft's magnetic field. The near field is defined as that part of the spacecraft's field that can not be satisfactorily represented by a centered dipole field. This region begins on the surface of the smallest sphere that completely encloses the spacecraft and extends outward until the spacecraft's field is considered "sufficiently dipolar." This transition from a nondipolar to a dipolar field is not at all well defined and frequently occurs at large distances from the spacecraft.

If, for some reason, measurements cannot be made in the far-field (dipolar) portion of the spacecraft's field, data must be taken in the near field. It is here that one lacks a satisfactory data analysis technique. The only techniques available for analysis in this portion of the field require data that are difficult if not impossible to obtain. Two such techniques are described in References 2 and 3, and the difficulties with both of them are obvious. Each requires data to be taken on some closed surface surrounding the spacecraft. Whether or not these data can even be obtained depends upon the particular spacecraft in question. However, even at best, data collection is tedious and time consuming. Also, it would be difficult to devise a data collection system with sufficient flexibility to deal with any type

of spacecraft. These are major drawbacks, rendering any near-field analysis technique requiring this type of data highly impractical.

The only points at which the spacecraft's field can easily be measured lie in a horizontal plane or on a vertical line, both of which pass through the center of the spacecraft. If one could calculate the spacecraft's dipole moment from these data, the near-field problem would be solved. Unfortunately, an exact determination of the dipole moment from this limited amount of data is, in principle, impossible. However, it was found that if an assumption were made about the nature of the field, the calculations could be done. The spacecraft's field can be assumed to be adequately approximated by the superposition of a certain number of multipole fields. If this assumption is made, a unique solution for the dipole moment exists. However, if the assumption is invalid, there will be an error present in the calculations. Therefore, this type of near-field analysis must also include a procedure by which one can determine the magnitude of this error. If this can be done, one can specify limits within which the true dipole moment must lie. Only then is the task complete.

This report presents a technique which satisfies the above requirements. In the interest of completeness, the theory is developed from first principles and carried through to final form. The accuracy of the method has been carefully evaluated by computer simulation of many sample cases. The results of these tests are discussed along with recommendations for the applications of this technique.

CHAPTER II

THEORETICAL CONSIDERATIONS

Magnetically, a spacecraft is a localized source containing macroscopic currents and magnetic matter that give rise to a magnetic field. This field obeys Maxwell's equations everywhere in space. The problem is to determine the form of this field in terms of the parameters of the source. There are several ways in which one can do this. The formalism which will be used here involves an expansion of the field in terms of known vector functions of the angular coordinates, and solution for the coefficients of this expansion by the use of Maxwell's equations. These vector functions are known as "vector spherical harmonics" and are most commonly found in the literature of quantum mechanics. They are, however, a purely mathematical formalism, useful also for describing classical fields. A discussion of them is included in Appendix A and only the directly relevant portions will be employed in the main text. It is necessary, however, to start with several preliminary definitions.

Throughout the text all functions will be referenced to a coordinate system whose origin, 0, is located somewhere within the source. The coordinates used will be either spherical polar or Cartesian (Figure 1). The vector spherical harmonic formalism requires the definition of so-called "spherical unit vectors." These vectors will be designated by $\mathbf{e}_{+1}$, $\mathbf{e}_0$, and $\mathbf{e}_{-1}$, and are defined as

$$\mathbf{e}_{+1} = -\frac{1}{\sqrt{2}}(\mathbf{u}_1 + i\mathbf{u}_2) ,$$

$$\mathbf{e}_0 = \mathbf{u}_3 ,$$

and

$$\mathbf{e}_{-1} = \frac{1}{\sqrt{2}}(\mathbf{u}_1 - i\mathbf{u}_2) ,$$

where $i = \sqrt{-1}$. These vectors have the following properties:

(1) The complex conjugate is given by

$$\mathbf{e}_j^* = (-1)^j \mathbf{e}_{-j} .$$

(2) The scalar product satisfies

$$\mathbf{e}_{q'}^* , \quad \mathbf{e}_q = \delta_{qq'} .$$

(3) Any vector can be expressed in terms of these unit vectors. The spherical components of a vector $\mathbf{V}$ are given by

$$V_j = \mathbf{e}_j \cdot \mathbf{V} , \quad j = \pm 1, 0 .$$

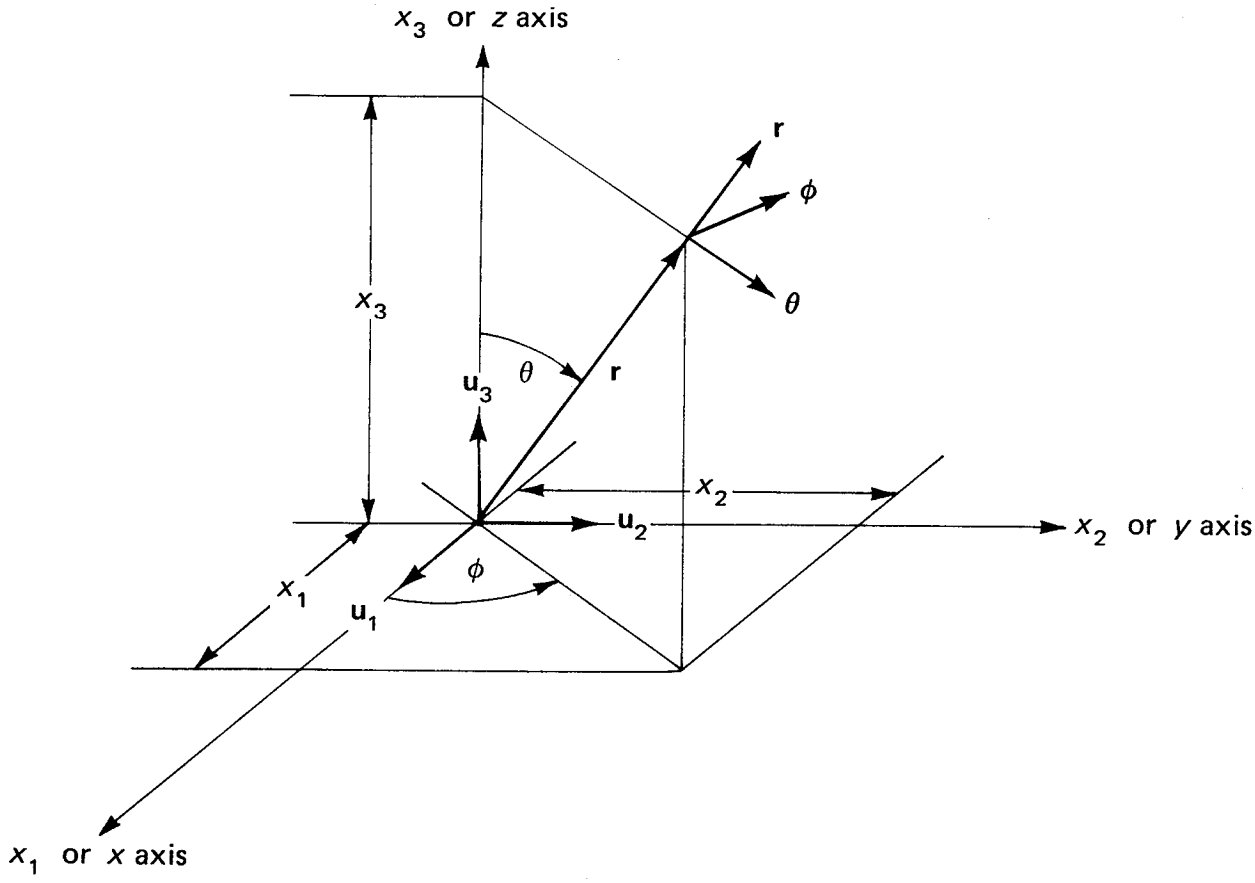

$$\mathbf{r} = \mathbf{u}_1 \cos\phi \sin\theta + \mathbf{u}_2 \sin\phi \sin\theta + \mathbf{u}_3 \cos\theta$$
$$\theta = \mathbf{u}_1 \cos\phi \cos\theta + \mathbf{u}_2 \sin\phi \cos\theta - \mathbf{u}_3 \sin\theta$$
$$\phi = -\mathbf{u}_1 \cos\phi + \mathbf{u}_2 \sin\phi$$

Figure 1—Coordinates of the position vector **r** in Cartesian and spherical polar coordinate systems.

If the spherical components of the vector are given, the vector appears as

$$\mathbf{V} = \sum_{j=-1}^{+1} (-1)^j V_j \mathbf{e}_{-j}$$

$$= \sum_{j=-1}^{+1} \mathbf{e}_j^* V_j \ .$$

In terms of the associated Legendre functions $p_j^m(\cos\theta)$, given by the equation

$$P_j^m(x) = \frac{(-1)^m}{2^j j!}(1-x^2)^{m/2}\left(\frac{d}{dx}\right)^{j+m}(x^2-1)^j \ , \tag{1}$$

ordinary spherical harmonics $Y_{jm}(\theta, \phi)$ can be defined by

$$Y_{jm}(\theta,\phi) = (-1)^m \sqrt{\frac{2j+1}{4\pi}\frac{(j-m)!}{(j+m)!}} P_j^m(\cos\theta) e^{im\phi} . \tag{2}$$

The vector spherical harmonics $\mathbf{Y}_{jk}^M(\theta,\phi)$ can now be defined as

$$\mathbf{Y}_{jk}^M(\theta,\phi) = \sum_{m=-k}^{+k} \sum_{q=-1}^{+1} Y_{km}(\theta,\phi) C_{k1}(J,M;m,q) \mathbf{e}_q , \tag{3}$$

where the quantities $C_{k1}(J,M;m,q)$ are known as Clebsch-Gordan coefficients.

The formulas for the coefficients appropriate to this discussion are given in Appendix A, Table A-1. They exhibit the property that $C_{k1} = 0$ unless $k = J \pm 1, J$ and $M = m + q$.

This means that for each value of J except $J = 0$ there will be three vector spherical harmonics. Since the functions Y_{km} form a complete set for scalar functions and the $\mathbf{e}_q$ are a complete set of basis vectors, the functions in Equation 3 also form a complete set for vector functions in three dimensions. Hence, any vector field may be written as a linear combination of the $\mathbf{Y}_{jk}^M$, with coefficients depending on the radial coordinate alone.

Let the steady-state current density distribution within the source be denoted by **J**(**r**) and the magnetization density by **M**(**r**). Let these sources give rise to a magnetic vector potential **A**(**r**) and a magnetic flux density **B**(**r**) related to it by $\mathbf{B} = \nabla \times \mathbf{A}$. According to the usual conventions, one defines the magnetic field strength **H**(**r**) by $\mathbf{H} = \mathbf{B}/\mu_0 - \mathbf{M}$ in rationalized MKS units. These functions then satisfy the following equations:

$$\nabla \times \mathbf{H}(\mathbf{r}) = \begin{cases} \mathbf{J}(\mathbf{r}) , & \text{inside} \\ 0 , & \text{outside} \end{cases} ,$$

$$\nabla \times \mathbf{B}(\mathbf{r}) = \begin{cases} \mu_0 \mathbf{J}(\mathbf{r}) + \mu_0 \nabla \times \mathbf{M}(\mathbf{r}) , & \text{inside} \\ 0 , & \text{outside} \end{cases} ,$$

and

$$\nabla \times \nabla \times \mathbf{A}(\mathbf{r}) = \begin{cases} \mu_0 \mathbf{J}(\mathbf{r}) + \mu_0 \nabla \times \mathbf{M}(\mathbf{r}) , & \text{inside} \\ 0 , & \text{outside} \end{cases} .$$

These equations are valid throughout all space. (Note that **J** and **M** are zero outside the source.)

If **A** and **B** are expanded in terms of the vector spherical harmonics,

$$\mathbf{A}(\mathbf{r}) = \sum_{j=0}^{\infty} \sum_{m=-j}^{+j} \sum_{k=-1}^{+1} d_k(j,m,r) \mathbf{Y}_{j,j+k}^m(\theta,\phi)$$

$$= \sum_{j=0}^{\infty} \sum_{m=-j}^{+j} \mathbf{A}_{jm}(\mathbf{r})$$

and

$$\mathbf{B}(\mathbf{r}) = \sum_{j=0}^{\infty} \sum_{m=-j}^{+j} \sum_{k=-1}^{+1} d'_k(j,m,r)\mathbf{Y}^m_{j,j+lc}(\theta,\phi)$$

$$= \sum_{j=0}^{\infty} \sum_{m=-j}^{+j} \mathbf{B}_{jm}(\mathbf{r}) .$$

The quantities $\mathbf{A}_{jm}$ and $\mathbf{B}_{jm}$ are known as "pure multipole fields".

Outside the source, one must require that

$$\nabla \cdot \mathbf{B}_{jm} = \nabla \times \mathbf{B}_{jm} = 0 .$$

Therefore (from Appendix A, Equations A-6, A-7, and A-8),

$$\nabla \cdot \mathbf{B}_{jm} = \left[\sqrt{\frac{j+1}{2j+1}} \left(\frac{d}{dr} + \frac{j+2}{r} \right) d'_{+1} + \sqrt{\frac{j}{2j+1}} \left(\frac{d}{dr} - \frac{j-1}{r} \right) d'_{-1} \right] Y_{jm} = 0$$

and, from $\nabla \times \mathbf{B}_{jm} = 0$,

$$\frac{i}{\sqrt{2j+1}} \left\{ \left[\sqrt{j} \left(\frac{d}{dr} + \frac{j+2}{r} \right) d'_{+1} + \sqrt{j+1} \left(\frac{d}{dr} - \frac{j-1}{r} \right) d'_{-1} \right] \mathbf{Y}^m_{jj} \right.$$

$$\left. + \sqrt{j} \left(\frac{d}{dr} - \frac{j}{r} \right) d'_0 \mathbf{Y}^m_{j,j+1} + \sqrt{j+1} \left(\frac{d}{dr} + \frac{j+1}{r} \right) d'_0 \mathbf{Y}^m_{j,j-1} \right\} = 0 .$$

Since the functions $\mathbf{Y}^m_{jk}$ and $\mathbf{Y}_{jm}$ are not zero, their coefficients must be. Hence,

$$\sqrt{j+1} \left(\frac{d}{dr} + \frac{j+2}{r} \right) d'_{+1} + \sqrt{j} \left(\frac{d}{dr} - \frac{j-1}{r} \right) d'_{-1} = 0 \tag{4}$$

and

$$j \left(\frac{d}{dr} + \frac{j+2}{r} \right) d'_{+1} + \sqrt{j+1} \left(\frac{d}{dr} - \frac{j-1}{r} \right) d'_{-1} = 0 , \tag{5}$$

so that

$$\left(\frac{d}{dr} - \frac{j}{r} \right) d'_0 = 0 \tag{6a}$$

and

$$\left(\frac{d}{dr} + \frac{j+1}{r} \right) d'_0 = 0 . \tag{6b}$$

The solution for Equations 6a and 6b exists only when $d'_0 = 0$. The solutions for Equations 4 and 5 exist when

$$\left(\frac{d}{dr} + \frac{j+2}{r} \right) d'_{+1} = \left(\frac{d}{dr} - \frac{j-1}{r} \right) d'_{-1} = 0 .$$

Therefore, one must require

$$d'_{+1} \approx r^{-j-2}$$

$$d'_{-1} \approx r^{j-1} \ .$$

In a region containing no sources, $\mathbf{B}_{jm}$ must therefore have the form

$$\mathbf{B}_{jm}(\mathbf{r}) = \frac{a}{r^{j+2}} \mathbf{Y}^m_{j,j+1}(\theta,\phi) + br^{j-1} \mathbf{Y}^m_{j,j-1}(\theta,\phi) \ , \tag{7}$$

where a and b are constants.

In order to give this form for $\mathbf{B}_{jm}$, the fields $\mathbf{A}_{jm}$ must be of the form

$$\mathbf{A}_{jm}(\mathbf{r}) = d_0(j,m,r)\mathbf{Y}^m_{jj}(\theta,\phi) \ . \tag{8}$$

This is so because $\nabla \times \mathbf{Y}^m_{j,j\pm1}$ leads to terms that contain the functions $\mathbf{Y}^m_{jj}$, which are not found in Equation 5. Hence, one is free to take $d_{\pm1}(j,m,r) = 0$.

In order to determine the quantity d_0 in Equation 8, the equation

$$\nabla \times [\nabla \times \mathbf{A}(\mathbf{r})] = \mu_0 \mathbf{J}(\mathbf{r}) + \mu_0 \nabla \times \mathbf{M}(\mathbf{r}) \tag{9}$$

must be solved. From Appendix A, Equations A-3, A-4, and A-5,

$$\nabla \times \mathbf{A}_{jm} = \frac{i}{\sqrt{2j+1}} \left[\sqrt{j} \left(\frac{d}{dr} - \frac{j}{r} \right) d_0 \mathbf{Y}^m_{j,j+1} + \sqrt{j+1} \left(\frac{d}{dr} + \frac{j+1}{r} \right) d_0 \mathbf{Y}^m_{j,j-1} \right] \ ,$$

and

$$\nabla \times (\nabla \times \mathbf{A}_{jm}) = -\frac{1}{2j+1} \left[j \left(\frac{d}{dr} + \frac{j+2}{r} \right) \left(\frac{d}{dr} - \frac{j}{r} \right) + (j+1) \left(\frac{d}{dr} - \frac{j-1}{r} \right) \left(\frac{d}{dr} + \frac{j+1}{r} \right) \right] d_0 \mathbf{Y}^m_{jj} \ .$$

Now,

$$\left(\frac{d}{dr} + \frac{j+2}{r} \right) \left(\frac{d}{dr} - \frac{j}{r} \right) = \left(\frac{d}{dr} - \frac{j-1}{r} \right) \left(\frac{d}{dr} + \frac{j+1}{r} \right) = \frac{d^2}{dr^2} + \frac{2}{r} \frac{d}{dr} - \frac{j(j+1)}{r^2} \ ,$$

as can easily be verified by expansion of the expressions in brackets. Hence,

$$\nabla \times (\nabla \times \mathbf{A}_{jm}) = -\left[\frac{d^2}{dr^2} + \frac{2}{r} \frac{d}{dr} - \frac{j(j+1)}{r^2} \right] d_0(j,m,r) \mathbf{Y}^m_{jj} = -\Delta(r)\, d_0(j,m,r) \mathbf{Y}^m_{jj} \ .$$

Therefore,

$$\nabla \times [\nabla \times \mathbf{A}(\mathbf{r})] = \sum_{j=0}^{\infty} \sum_{m=-j}^{+j} -\Delta(r)\, d_0(j,m,r) \mathbf{Y}_{jj}(\theta,\phi) = \mu_0 \mathbf{J}(\mathbf{r}) + \mu_0 \nabla \times \mathbf{M}(\mathbf{r}) \ .$$

Since

$$\int [\mathbf{Y}^m_{jk}(\theta,\phi)]^* \cdot [\mathbf{Y}^{m'}_{j'k'}(\theta,\phi)]\, d\Omega = \delta_{jj'}\, \delta_{kk'}\, \delta_{mm'} \ ,$$

the following equation for $d_0(j,m,r)$ is obtained:

$$\left(\frac{d^2}{dr^2} + \frac{2}{r}\frac{d}{dr} - \frac{j(j+1)}{r^2}\right) d_0(j,m,r) = -\mu_0 \int [\mathbf{Y}_{jj}^m(\theta',\phi')]^* \cdot [\mathbf{J}(\mathbf{r}') + \nabla \times \mathbf{M}(\mathbf{r}')]\, d\Omega(\mathbf{r}')$$

$$= -K(j,m,r)\,. \tag{10}$$

The function d_0 can now be obtained with the use of Green's functions. Consider the operator Δ given by

$$\Delta(r) = \frac{d^2}{dr^2} + \frac{2}{r}\frac{d}{dr} - \frac{j(j+1)}{r^2}$$

$$= \frac{1}{r^2}\frac{d}{dr}\left(r^2 \frac{d}{dr}\right) - \frac{j(j+1)}{r}\,.$$

Consider the integral

$$I = \int_0^\infty g(\Delta f) r^2\, dr$$

$$= \int_0^\infty g \frac{d}{dr}\left(r^2 \frac{d}{dr} f\right) dr - j(j+1) \int_0^\infty gf\, dr\,.$$

If this is integrated by parts twice,

$$I = gr^2 \frac{d}{dr} f \Big|_0^\infty - fr^2 \frac{d}{dr} g \Big|_0^\infty + \int_0^\infty f \frac{d}{dr}\left(r^2 \frac{d}{dr} g\right) dr - j(j+1) \int_0^\infty gf\, dr\,. \tag{11}$$

If f and g are required to approach zero faster than $1/r$ as r approaches infinity, and if they are not infinite at $r = 0$, the first two terms disappear, and

$$\int_0^\infty g(\Delta f) r^2\, dr = \int_0^\infty f(\Delta g) r^2\, dr\,. \tag{12}$$

Now, if the solution to the equation

$$\Delta(r) g(r,r') = \frac{\delta(r-r')}{r^2} \tag{13}$$

were known, the solution to the arbitrary equation

$$\Delta(r) f(r) = f'(r) \tag{14}$$

could be found as follows: Multiply Equation 14 by $r^2 g(r,r')$ and integrate, so that

$$\int_0^\infty r^2 g(r,r')\,[\Delta(r)f(r)]\;dr = \int_0^\infty g(r,r')f'(r)r^2\;dr\;.$$

By Equation 12, this reduces to

$$\int_0^\infty r^2 f(r)[\Delta(r)g(r,r')]\;dr = \int_0^\infty f(r)\delta(r-r')\;dr$$

$$= f(r')\;.$$

Hence, the solution to Equation 14 is

$$f(r') = \int_0^\infty g(r,r')f(r)r^2\;dr\;.$$

Therefore, the solution to Equation 13 is needed.

If $r = r'$,

$$\left[\frac{d^2}{dr^2} + \frac{2}{r}\frac{d}{dr} - \frac{j(j+1)}{r^2}\right] g_j(r,r') = 0\;.$$

The solutions are

$$g_j(r,r') = \begin{cases} Ar^j + A'r^{-(j+1)} \text{ for } r < r' \\ B'r^j + Br^{-(j+1)} \text{ for } r > r' \end{cases}\;.$$

The boundary conditions on g are, from Equation 11, g_j approaches zero as r approaches infinity and g_j approaches infinity as r approaches zero. Therefore, $A' = B' = 0$ and

$$g_j(r,r') = \begin{cases} Ar^j \text{ for } r < r' \\ Br^{-(j+1)} \text{ for } r > r' \end{cases}\;.$$

This can be written as

$$g_j(r,r') = C\frac{r_<^j}{r_>^{j+1}}\;,$$

where $r_>$ denotes the greater of r and r' and $r_<$ denotes the lesser of r and r'. The constant C can now be determined so that the slope of g_j has the correct discontinuity at $r = r'$.

If one integrates Equation 9 from $r = r' - \epsilon$ to $r = r' + \epsilon$ and allows ϵ to approach zero, the value for C will have been determined:

$$\lim_{\epsilon \to 0} \left[\int_{r'-\epsilon}^{r'+\epsilon} \frac{d}{dr} r^2 \frac{d}{dr} g_j(r,r')\, dr - j(j+1) \int_{r'-\epsilon}^{r'+\epsilon} g_j(r,r')\, dr \right] = \int_{r'-\epsilon}^{r'+\epsilon} \delta(r-r')\, dr$$

$$= 1 ,$$

$$\lim_{\epsilon \to 0} \left[r^2 \frac{d}{dr} g_j(r,r') \Big|_{r'+\epsilon} - r^2 \frac{d}{dr} g_j(r,r') \Big|_{r'-\epsilon} \right] = 1 ,$$

$$\lim_{\epsilon \to 0} \frac{d}{dr} g_j(r,r') \Big|_{r'+\epsilon} = -(j+1) C \left(\frac{1}{r'} \right)^2 ,$$

and

$$\lim_{\epsilon \to 0} \frac{d}{dr} g_j(r,r') \Big|_{r'-\epsilon} = jC \left(\frac{1}{r'} \right)^2 .$$

Therefore,

$$C = -\frac{1}{2j+1} .$$

Hence,

$$g_j(r,r') = -\frac{1}{2j+1} \frac{r_<^j}{r_>^{j+1}} ,$$

and the solution to Equation 10 can be written as

$$d_0(j,m,r) = \frac{1}{2j+1} \int_0^\infty \frac{r_<^j}{r_>^{j+1}} K(j,m,r') r'^2\, dr'$$

$$= \frac{\mu_0}{2j+1} \int_0^\infty \frac{r_<^j}{r_>^{j+1}} \int [\mathbf{Y}_{jj}^m]^* \cdot [\mathbf{J}(\mathbf{r}') + \nabla \times \mathbf{M}(\mathbf{r}')]\, d\Omega\, r'^2\, dr' .$$

Outside the source, $r > r'$ always; hence,

$$d_0(j,m,r) = \frac{1}{r^{j+1}} \frac{\mu_0}{2j+1} \int r'^j [\mathbf{Y}_{jj}^m(\theta',\phi)]^* \cdot [\mathbf{J}(\mathbf{r}') + \nabla \times \mathbf{M}(\mathbf{r}')]\, dV,$$

where dV is an element of volume defined by $r'^2\, dr'\, d\Omega$. Now, the solution for $\mathbf{A}(\mathbf{r})$ is

$$\mathbf{A}(\mathbf{r}) = \sum_{j=0}^{\infty} \sum_{m=-j}^{+j} \frac{D_{jm}}{2j+1} \mathbf{Y}_{jj}^m(\theta,\phi) \frac{1}{r^{j+1}} ,$$

where

$$D_{jm} = \mu_0 \int r'^{j} [\mathbf{Y}_{jj}^{m}(\theta',\phi')]^{*} \cdot [\mathbf{J}(\mathbf{r}') + \nabla \times \mathbf{M}(\mathbf{r}')]\, dV .$$

The magnetic flux density $\mathbf{B}(\mathbf{r})$ and the magnetic field $\mathbf{H}(\mathbf{r})$ outside the source are obtainable from the relation $\mu_0 \mathbf{H}(r) = \mathbf{B}(\mathbf{r}) = \nabla \times \mathbf{A}(\mathbf{r})$. Hence, from Equation A-5, Appendix A,

$$\mathbf{B}(\mathbf{r}) = \sum_{j=1}^{\infty} \sum_{m=-j}^{+j} -i\sqrt{\frac{j}{2j+1}}\, D_{jm} \mathbf{Y}_{j,j+1}^{m}(\theta,\phi) \frac{1}{r^{j+2}} ,$$

which is of the form of Equation 7 with $b = 0$.

Using Equation A-10, Appendix A, one may write

$$\frac{1}{r^{j+2}} \mathbf{Y}_{j,j+1}^{m}(\theta,\phi) = [(2j+1)(j+1)]^{-1/2} \nabla \left[\frac{1}{r^{j+1}} \mathbf{Y}_{jm}(\theta,\phi) \right] .$$

Hence,

$$\mathbf{B}(\mathbf{r}) = -\nabla \sum_{j=1}^{\infty} \sum_{m=-j}^{+j} i\sqrt{\frac{j}{j+1}}\, \frac{D_{jm}}{2j+1}\, \frac{Y_{jm}(\theta,\phi)}{r^{j+1}}$$

$$= -\nabla\, U(\mathbf{r}) .$$

The term D_{jm} may now be reduced to a more convenient form. Consider the integral

$$\int [\mathbf{Y}_{jj}^{m}(\theta,\phi)]^{*} \cdot \mathbf{V}\, d\Omega ,$$

where $\mathbf{V}$ is an arbitrary vector. From Equation A-9, Appendix A,

$$\mathbf{Y}_{jj}^{m}(\theta,\phi) = \frac{\mathbf{L} Y_{jm}(\theta,\phi)}{\sqrt{j(j+1)}} ,$$

where $\mathbf{L} = -i\mathbf{r} \times \nabla$. Then,

$$I = \int [\mathbf{L}^{*} Y_{jm}^{*}(\theta,\phi)] \cdot \mathbf{V}\, d\Omega .$$

In the spherical vector notation,

$$\mathbf{V}_1^{*} \cdot \mathbf{V}_2 = \sum_{j=-1}^{+1} \mathbf{V}_{ij}^{*} \mathbf{V}_{2j} .$$

Hence,

$$I = \int [(L_{+1}^{*} Y_{jm}^{*}) V_{+1} + (L_{-1}^{*} Y_{jm}^{*}) V_{-1} + (L_0^{*} Y_{jm}^{*}) V_0]\, d\Omega .$$

Now,

$$L_{+1} = -\frac{1}{\sqrt{2}}(L_x + iL_y)$$

$$= \frac{e^{i\phi}}{\sqrt{2}}\left(\frac{\partial}{\partial\theta} + i\cot\theta\,\frac{\partial}{\partial\phi}\right).$$

$$L_{-1} = \frac{1}{\sqrt{2}}(L_x - iL_y)$$

$$= -\frac{e^{i\phi}}{\sqrt{2}}\left(\frac{\partial}{\partial\theta} - i\cot\theta\,\frac{\partial}{\partial\phi}\right),$$

and

$$L_0 = L_z$$

$$= -i\frac{\partial}{\partial\theta},$$

so that

$$I_{+1} = \int (L^*_{+1} Y^*_{jm}) V_{+1}\, d\Omega$$

$$= -\frac{1}{\sqrt{2}}\int e^{+i\phi}\left[\left(\frac{\partial}{\partial\theta} - i\cot\theta\,\frac{\partial}{\partial\phi}\right)Y^*_{jm}\right] V_{+1}\sin\theta\, d\theta\, d\phi.$$

Integrating by parts yields

$$I_{+1} = -\frac{1}{\sqrt{2}}\sin\theta\int_0^{2\pi} e^{-i\phi}\, Y^*_{jm}(\theta,\phi) V_{+1}\, d\phi\Bigg|_0^{\pi}$$

$$+ C_{jm}\frac{e^{-2i\phi}}{\sqrt{2}}\int_0^{\pi}\cos\theta\, P_j^m(\cos\theta) V_{+1}\, d\theta\Bigg|_0^{2\pi}$$

$$+ \frac{1}{\sqrt{2}}\int Y^*_{jm}(\theta,\phi)\frac{\partial}{\partial\theta}(\sin\theta\, V_{+1}) e^{-i\phi}\, d\theta\, d\phi$$

$$- \frac{i}{\sqrt{2}}\int Y^*_{jm}(\theta,\phi)\cos\theta\,\frac{\partial}{\partial\phi}(V_{+1} e^{-i\phi})\, d\theta\, d\phi.$$

Since the first two terms are equal to zero,

$$I_{+1} = \frac{1}{\sqrt{2}} \int Y^*_{jm}(\theta,\phi) e^{-i\phi} \left[\left(\frac{\partial}{\partial\theta} - i \cot\theta \frac{\partial}{\partial\phi} \right) V_{+1} \right] \sin\theta \, d\theta \, d\phi$$

$$+ \frac{1}{\sqrt{2}} \int Y^*_{jm}(\theta,\phi) V_{+1} (\cos\theta \, e^{-i\phi} - \cos\theta \, e^{-i\phi}) \, d\theta \, d\phi$$

$$= - \int Y^*_{jm}(\theta,\phi)(L^*_{+1} \, V_{+1}) \, d\Omega \, .$$

Similarly,

$$I_{-1} = \int [L^*_{-1} Y^*_{jm}(\theta,\phi)] \, V_{-1} \, d\Omega$$

$$= - \int Y^*_{jm}(\theta,\phi)(L^*_{-1} \, V_{-1}) \, d\Omega$$

and

$$I_0 = \int V_0 \, [L^*_0 \, Y^*_{jm}(\theta,\phi)] \, d\Omega$$

$$= \int Y^*_{jm}(\theta,\phi)(L^*_0 \, V_0) \, d\Omega \, .$$

Therefore,

$$I = \int Y^*_{jm}(\theta,\phi)(-L^*_{+1} \, V_{+1} - L^*_{-1} \, V_{-1} + L_0 \, V_0) \, d\Omega$$

$$= - \int \mathbf{Y}^*_{jm}(\theta,\phi) \mathbf{L}^* \cdot \mathbf{V} \, d\Omega$$

$$= \int Y^*_{jm}(\theta,\phi) \, \mathbf{L} \cdot \mathbf{V} \, d\Omega \, .$$

Hence,

$$\int (\mathbf{Y}^m_{ji})^* \cdot \mathbf{V} \, d\Omega = \frac{1}{\sqrt{j(j+1)}} \int Y^*_{jm} (\mathbf{L} \cdot \mathbf{V}) \, d\Omega \, ,$$

so that

$$D_{jm} = \frac{\mu_0}{\sqrt{j(j+1)}} \int r^j Y^*_{jm}(\theta,\phi)[\mathbf{L} \cdot \mathbf{J}(\mathbf{r}) + \mathbf{L} \cdot \nabla \times \mathbf{M}(\mathbf{r})]\, dV .$$

This can be reduced further; consider

$$(\mathbf{r} \times \nabla) \cdot \mathbf{J} = \left(x_2 \frac{\partial}{\partial x_3} - x_3 \frac{\partial}{\partial x_2}\right) J_1 + \left(x_3 \frac{\partial}{\partial x_1} - x_1 \frac{\partial}{\partial x_3}\right) J_2 + \left(x_1 \frac{\partial}{\partial x_2} - x_2 \frac{\partial}{\partial x_1}\right) J_3$$

$$= x_1 \left(\frac{\partial}{\partial x_2} J_3 - \frac{\partial}{\partial x_3} J_2\right) + x_2 \left(\frac{\partial}{\partial x_3} J_1 - \frac{\partial}{\partial x_1} J_3\right) + x_3 \left(\frac{\partial}{\partial x_1} J_2 - \frac{\partial}{\partial x_2} J_1\right)$$

$$= \mathbf{r} \cdot (\nabla \times \mathbf{J})$$

$$= \mathbf{J} \cdot (\nabla \times \mathbf{r}) - \nabla \cdot (\mathbf{r} \times \mathbf{J}) .$$

Since $\nabla \times \mathbf{r} = 0$, one can write

$$\mathbf{L} \cdot \mathbf{J} = i \nabla \cdot (\mathbf{r} \times \mathbf{J}) .$$

Now consider $\mathbf{L} \cdot (\nabla \times \mathbf{M})$. By the previous equation,

$$\mathbf{L} \cdot (\nabla \times \mathbf{M}) = i \nabla \cdot [\mathbf{r} \times (\nabla \times \mathbf{M})]$$

$$= i \nabla \cdot [\nabla(\mathbf{r} \cdot \mathbf{M}) - \mathbf{M} \times (\nabla \times \mathbf{r}) - (\mathbf{r} \cdot \nabla)\mathbf{M} - (\mathbf{M} \cdot \nabla)\mathbf{r}]$$

$$= i [\nabla^2 (\mathbf{r} \cdot \mathbf{M}) - \nabla \cdot [(\mathbf{r} \cdot \nabla)\mathbf{M}] - \nabla \cdot \mathbf{M}] .$$

Now,

$$\nabla \cdot [(\mathbf{r} \cdot \nabla)\mathbf{M}] = \sum_{j=1}^{3} \frac{\partial}{\partial x_j} \left(\sum_{k=1}^{3} x_k \frac{\partial}{\partial x_k}\right) M_j$$

$$= \sum_{jk} \left(\delta_{jk} \frac{\partial}{\partial x_k} M_j + x_k \frac{\partial}{\partial x_k} \frac{\partial}{\partial x_j} M_j\right)$$

$$= \nabla \cdot \mathbf{M} + (\mathbf{r} \cdot \nabla)(\nabla \cdot \mathbf{M}) .$$

Hence,

$$\mathbf{L} \cdot (\nabla \times \mathbf{M}) = - i [-\nabla^2 (\mathbf{r} \cdot \mathbf{M}) + (\mathbf{r} \cdot \nabla + 2) \nabla \cdot \mathbf{M}] .$$

Therefore,

$$D_{jm} = \frac{\mu_0 i}{\sqrt{j(j+1)}} \left\{ \int r^j Y^*_{jm}(\theta,\phi)[\nabla \cdot (\mathbf{r} \times \mathbf{J})]\, dV - \int r^j Y^*_{jm}(\theta,\phi)(\mathbf{r} \cdot \nabla + 2)(\nabla \cdot \mathbf{M})\, dV \right.$$

$$\left. + \int r^j Y^*_{jm}(\theta,\phi) \nabla^2 (\mathbf{r} \cdot \mathbf{M})\, dV \right\} .$$

The last integral vanishes upon integration by parts, since $\nabla^2 r^j Y^*_{jm}(\theta,\phi) = 0$. The second integral can also be evaluated by integration by parts. The result is

$$\int_0^\infty r^j(\mathbf{r}\cdot\nabla + 2)(\nabla\cdot\mathbf{M})r^2\,dr = -(j+1)\int r^j \nabla\cdot\mathbf{M}\, r^2\,dr\,.$$

Hence,

$$D_{jm} = \frac{\mu_0 i}{\sqrt{j(j+1)}}\int r^j Y^*_{jm}(\theta,\phi)\,\nabla\cdot[\mathbf{r}\times\mathbf{J} + (j+1)\mathbf{M}]\,dV\,.$$

The magnetic flux density can now be written as

$$\mathbf{B}(\mathbf{r}) = -\nabla\sum_{j=1}^{\infty}\sum_{m=-j}^{+j}\frac{-\mu_0}{2j+1}\int r^j Y^*_{jm}(\theta,\phi)\nabla\cdot\left(\frac{\mathbf{r}\times\mathbf{J}}{j+1} + \mathbf{M}\right)dV\,\frac{Y_{jm}(\theta,\phi)}{r^{j+1}}$$

$$= -\nabla U(\mathbf{r})\,.$$

It is now convenient to write this field in terms of real quantities.

From the definition of Y_{jm},

$$Y_{j,-m}(\theta,\phi) = (-1)^m Y_{jm}(\theta,\phi)\,.$$

Then, if

$$Q_{jm} = \int Y^*_{jm}(\theta',\phi')f(r')\,dV\,Y_{jm}(\theta,\phi)$$

and

$$Q_{j,-m} = Q^*_{jm}\,,$$

we have

$$\sum_{m=-j}^{+j} Q_{jm} = Q_{j0} + \sum_{m=+1}^{j}(Q_{jm} + Q^*_{jm})\,.$$

Now,

$$Y_{jm}(\theta,\phi) = \sqrt{\frac{2j+1}{4\pi}\,\frac{(j-m)!}{(j+m)!}}\,P_j^m(\cos\theta)e^{im\phi} = C_{jm}P_j^m e^{im\phi}\,.$$

Therefore,

$$Q_{jm} + Q^*_{jm} = C^2_{jm}\left[\int P_j^m(\cos\theta')\cos m\phi' f(r')\,dV\,P_j^m(\cos\theta)\cos m\phi\right.$$

$$\left. + \int P_j^m(\cos\theta')\sin m\phi' f(r')\,dV\,P_j^m(\cos\theta)\cos m\phi\right]\,.$$

One can now write

$$\mathbf{B}(\mathbf{r}) = -\frac{\mu_0}{4\pi}\nabla\sum_{j=1}^{\infty}\sum_{m=0}^{j}(a_{jm}\cos m\phi + b_{jm}\sin m\phi)\frac{P_j^m(\cos\theta)}{r^{j+1}}\,, \tag{15}$$

where

$$a_{jm} = -(2-\delta_{jo})\frac{(j-m)!}{(j+m)!}\int r^j P_j^m(\cos\theta)\cos m\phi\,\nabla\cdot\left[\frac{\mathbf{r}\times\mathbf{J}(\mathbf{r})}{j+1} + \mathbf{M}(\mathbf{r})\right]dV \tag{16a}$$

and

$$b_{jm} = -2\frac{(j-m)!}{(j+m)!}\int r^j P_j^m(\cos\theta)\sin m\phi\,\nabla\cdot\left[\frac{\mathbf{r}\times\mathbf{J}(\mathbf{r})}{j+1} + \mathbf{M}(\mathbf{r})\right]dV\,. \tag{16b}$$

These quantities will be known as multipole moment coefficients.

Consider now the lowest order term in Equation 15; call this term $\mathbf{B}_1$:

$$\begin{aligned}\mathbf{B}_1 &= -\frac{\mu_0}{4\pi}\nabla\left[a_{10}P_1^0 + (a_{11}\cos\phi + b_{11}\sin\phi)P_1^1\right]\frac{1}{r^2}\\ &= -\frac{\mu_0}{4\pi}\nabla\left[a_{10}\cos\theta + a_{11}\sin\theta\cos\phi + b_{11}\sin\theta\sin\phi\right]\frac{1}{r^2}\\ &= -\frac{\mu_0}{4\pi}\nabla\left(\frac{\mathbf{m}\cdot\mathbf{r}}{r^3}\right)\,,\end{aligned}$$

where $\mathbf{m}$ is the vector whose components are a_{11}, b_{11}, and a_{10}. Using Equations 6a and 6b, one can now write

$$\mathbf{m} = \int \mathbf{r}\left\{\nabla\cdot\left[\frac{1}{2}\mathbf{r}\times\mathbf{J}(\mathbf{r}) + \mathbf{M}(\mathbf{r})\right]\right\}dV\,.$$

This vector is defined as the dipole moment of the system. By Gauss' law,

$$\int \mathbf{r}\left\{\nabla\cdot\left[\frac{1}{2}\mathbf{r}\times\mathbf{J}(\mathbf{r}) + \mathbf{M}(\mathbf{r})\right]\right\}dV = \int_{\text{surface}} \mathbf{r}\left[\frac{1}{2}\mathbf{r}\times\mathbf{J}(\mathbf{r}) + \mathbf{M}(\mathbf{r})\right]\cdot d\mathbf{s} + \int_{\text{volume}}\left\{\left[\frac{1}{2}\mathbf{r}\times\mathbf{J}(\mathbf{r}) + \mathbf{M}(\mathbf{r})\right]\cdot\nabla\right\}\mathbf{r}\,dV$$

$$= -\int\left[\frac{1}{2}\mathbf{r}\times\mathbf{J}(\mathbf{r}) + \mathbf{M}(\mathbf{r})\right]dV\,.$$

The last form is obtained because the first integral is equal to zero and $(\mathbf{A}\cdot\nabla)\mathbf{r} = \mathbf{A}$ in the second integral. Hence,

$$\mathbf{m} = \int\left[\frac{1}{2}\mathbf{r}\times\mathbf{J}(\mathbf{r}) + \mathbf{M}(\mathbf{r})\right]dV\,.$$

The significance of this quantity can be understood from the following discussion. Consider an element of current density $\mathbf{J}\,dV$ and an element of magnetization $\mathbf{M}\,dV$ in a uniform magnetic induction $\mathbf{B}$. The torque on the current element is given by

$$\begin{aligned} d\mathbf{N}_J &= \mathbf{r} \times [\mathbf{J}(\mathbf{r})\,dV \times \mathbf{B}] \\ &= \mathbf{r} \times [\mathbf{J}(\mathbf{r}) \times \mathbf{B}]\,dV\,, \end{aligned}$$

and the torque on the magnetic material is given by

$$d\mathbf{N}_M = \mathbf{M}(\mathbf{r}) \times \mathbf{B}\,dV\,.$$

The total torque is given by an integral over the entire source:

$$\begin{aligned} \mathbf{N} &= \int d\mathbf{N}_J + \int d\mathbf{N}_M \\ &= \int \mathbf{r} \times [\mathbf{J}(\mathbf{r}) \times \mathbf{B}] \times \mathbf{M}(\mathbf{r}) \times \mathbf{B} \Big\}\, dV \\ &= \int \mathbf{J}(\mathbf{r})(\mathbf{r} \cdot \mathbf{B})\,dV + \mathbf{B}\int \mathbf{r} \cdot \mathbf{J}(\mathbf{r})\,dV + \int \mathbf{M}(\mathbf{r}) \times \mathbf{B}\,dV\,. \end{aligned}$$

Now,

$$\int \mathbf{r} \cdot \mathbf{J}(\mathbf{r})\,dV = \frac{1}{2}\int [\mathbf{J}(\mathbf{r}) \cdot \nabla]\, r^2\,dV\,.$$

If this is integrated by parts,

$$\int [\mathbf{J}(\mathbf{r}) \cdot \nabla]\, r^2\,dV = \int_{\text{surface}} r^2\,\mathbf{J}(\mathbf{r}) \cdot d\mathbf{s} - \int_{\text{volume}} r^2\,[\nabla \cdot \mathbf{J}(\mathbf{r})]\,dV\,. \tag{17}$$

The first integral is equal to zero since the current is localized, and the second integral is equal to zero since the current is stationary (i.e., $\nabla \cdot \mathbf{J} = 0$). Hence,

$$\mathbf{N} = \int [\mathbf{J}(\mathbf{r})(\mathbf{r} \cdot \mathbf{B}) + \mathbf{M}(\mathbf{r}) \times \mathbf{B}]\,dV\,.$$

Consider

$$I = \int \mathbf{J}(\mathbf{r})(\mathbf{r} \cdot \mathbf{B})\,dV\,.$$

This can be rewritten in a more complicated form:

$$I = \int \left[\mathbf{J}(\mathbf{B} \cdot \mathbf{r}) - \frac{1}{2}\mathbf{r}(\mathbf{B} \cdot \mathbf{J}) + \frac{1}{2}\mathbf{r}(\mathbf{B} \cdot \mathbf{J}) \right] dV$$

$$= \frac{1}{2}\int \mathbf{J}(\mathbf{B} \cdot \mathbf{r}) - \mathbf{r}(\mathbf{B} \cdot \mathbf{J})\, dV + \frac{1}{2}\int \mathbf{r}(\mathbf{B} \cdot \mathbf{J}) + \mathbf{J}(\mathbf{B} \cdot \mathbf{r})\, dV$$

$$= -\frac{1}{2}\int \mathbf{B} \times (\mathbf{r} \times \mathbf{J})\, dV + \frac{1}{2}\int \mathbf{r}(\mathbf{B} \cdot \mathbf{J}) + \mathbf{J}(\mathbf{B} \cdot \mathbf{r})\, dV .$$

The second integral can be shown to be equal to zero by the following argument. The ith Cartesian component of this integral is

$$\sum_{j=1}^{3} \int x_i(B_j J_j) + J_i(B_j x_j)\, dV = \sum_{j=1}^{3} B_j \int (x_i J_j + J_i x_j)\, dV .$$

Now,

$$\nabla x_j = \mathbf{u}_j .$$

Therefore,

$$\sum_{j=1}^{3} B_j \int (x_i J_j + J_i x_j)\, dV = \sum_{j=1}^{3} B_j \int \mathbf{J} \cdot (x_i \nabla x_j + x_j \nabla x_i)\, dV$$

$$= \sum_{j=1}^{3} B_j \int \mathbf{J} \cdot \nabla x_i x_j\, dV$$

$$= \sum_{j=1}^{3} B_j \left(\int_{\text{surface}} x_i x_j \mathbf{J} \cdot d\mathbf{s} - \int_{\text{volume}} x_i x_j \nabla \cdot \mathbf{J}\, dV \right).$$

Both of the above integrals are zero by the same arguments as for Equation 17. Hence,

$$\mathbf{N} = -\frac{1}{2}\int \mathbf{B} \times [\mathbf{r} \times \mathbf{J}(\mathbf{r})]\, dV + \int \mathbf{M}(\mathbf{r}) \times \mathbf{B}\, dV$$

$$= \left(\int \left\{ \frac{1}{2}[\mathbf{r} \times \mathbf{J}(\mathbf{r})] + \mathbf{M}(\mathbf{r}) \right\} dV \right) \times \mathbf{B}$$

$$= \mathbf{m} \times \mathbf{B} .$$

Therefore, in a uniform field, the torque acts only on the dipole moment of the system. If the dipole moment of the system is known, the torque to be expected in a given field can be computed.

CHAPTER III

ANALYSIS OF THE MAGNETIC FIELD

Construction of the Near-Field Equations

It is now necessary to restrict the analysis to the problem at hand. That is, it will be assumed from now on that the magnetic field is known only at discrete points in space. The coordinates of the ith point are restricted by

$$\theta_i = 0, \pi/2, \pi ,$$

$$r_{\min} \leqslant r \leqslant r_{\max},$$

and

$$0 \leqslant \phi_i \leqslant 2\pi .$$

Here, $r_{\min}$ and $r_{\max}$ specify the limitations on the radial coordinate and are determined for each specific case by physical limitations. The measurement of the magnetic field is usually accomplished by rotating the source about the z-axis past a set of fixed magnetometer probes. The axes of these probes are aligned with the Cartesian axis of the coordinate system. It therefore makes sense to speak of the components of the magnetic field that are seen on the sensors rather than the spherical polar components. Let us now examine these components in more detail and develop the procedure by which the quantities of interest (a_{11}, b_{11}, and a_{10}) may be determined.

From Equation 15, the form the components must exhibit can be determined. The procedure is to perform first the gradient operation and then, for each value of $\theta(0, \pi/2, \pi)$, make the appropriate transformation of unit vectors. These transformations are—

$\theta = 0$	$\theta = \pi/2$	$\theta = \pi$
$\mathbf{r} = \mathbf{u}_3$	$\mathbf{r} = \mathbf{u}_1$	$\mathbf{r} = -\mathbf{u}_3$
$\theta = \mathbf{u}_1$	$\theta = -\mathbf{u}_3$	$\theta = -\mathbf{u}_1$
$\phi = \mathbf{u}_2$	$\phi = \mathbf{u}_2$	$\phi = \mathbf{u}_2$

Let $B_j(r, \phi, \cos\theta)$ designate the component parallel to $\mathbf{u}_j$ for a given probe location. For $\theta = \pi/2$,

$$B_1(r,\phi,0) = \frac{\mu_0}{4\pi} \sum_{j=1}^{\infty} \sum_{m=0}^{j} \frac{j+1}{r^{j+2}} (a_{jm} \cos m\phi + b_{jm} \sin m\phi) P_j^m(0) , \tag{18a}$$

$$B_2(r,\phi,0) = \frac{\mu_0}{4\pi}\sum_{j=1}^{\infty}\sum_{m=0}^{j}\frac{m}{r^{j+2}}(a_{jm}\sin m\phi - b_{jm}\cos m\phi)P_j^m(0)\,, \tag{18b}$$

and

$$B_3(r,\phi,0) = \frac{\mu_0}{4\pi}\sum_{j=1}^{\infty}\sum_{m=0}^{j}\frac{1}{r^{j+2}}(a_{jm}\cos m\phi + b_{jm}\sin m\phi)\frac{\partial}{\partial\theta}P_j^m(0)\,. \tag{18c}$$

For $\theta = 0$ and $\theta = \pi$, the equations are a bit simpler, since at these angles $\partial P_j^m/\partial\theta$ and $P_j^m/\sin\theta$ are equal to zero unless $m = 1$, and the P_j^m are equal to zero unless $m = 0$. Therefore, for $\theta = 0$,

$$B_1(r,\phi,1) = \frac{\mu_0}{4\pi}\sum_{j=1}^{\infty}\frac{-1}{r^{j+2}}(a_{j1}\cos\phi + b_{j1}\sin\phi)\frac{\partial}{\partial\theta}P_j^1(1)\,, \tag{19a}$$

$$B_2(r,\phi,1) = \frac{\mu_0}{4\pi}\sum_{j=1}^{\infty}\frac{1}{r^{j+2}}(a_{j1}\sin\phi - b_{j1}\cos\phi)\frac{P_j^1(1)}{\sin 0}\,, \tag{19b}$$

and

$$B_3(r,\phi,1) = \frac{\mu_0}{4\pi}\sum_{j=1}^{\infty}\frac{j+1}{r^{j+2}}a_{j0}P_j^0(1)\,. \tag{19c}$$

For $\theta = \pi$,

$$B_1(r,\phi,-1) = \frac{\mu_0}{4\pi}\sum_{j=1}^{\infty}\frac{1}{r^{j+2}}(a_{j1}\cos\phi + b_{j1}\sin\phi)\frac{\partial}{\partial\theta}P_j^1(-1)\,, \tag{20a}$$

$$B_2(r,\phi,-1) = \frac{\mu_0}{4\pi}\sum_{j=1}^{\infty}\frac{1}{r^{j+2}}(a_{j1}\sin\phi - b_{j1}\cos\phi)\frac{P_j^1(-1)}{\sin\pi}\,, \tag{20b}$$

and

$$B_3(r,\phi,-1) = \frac{\mu_0}{4\pi}\sum_{j=1}^{\infty}\frac{-(j+1)}{r^{j+2}}a_{j0}P_j^0(-1)\,. \tag{20c}$$

Notice now that a Fourier analysis can create two uncoupled sets of simultaneous equations for each value of the index m (except $m = 0$, for which there is only one set). For a given value of m, each set will involve all the coefficients having that value of m for which $j \geq m$. We are interested only in the three sets involving the dipole-moment components. The sets involving the coefficients a_{11} and b_{11} are related only to the fundamental sine and cosine amplitudes of the components B_1 and B_2 on each probe. The set involving a_{10} is related to the dc amplitude of the B_3 components.

In a Fourier series, the amplitude A_m of the sin $m\phi$ term in the function $B(\phi)$ is given by

$$A_m = \frac{1}{\pi}\int_0^{2\pi} B(\phi)\sin m\phi \, d\phi \, .$$

The amplitude of the cos $m\phi$ term is similar, with sin $m\phi$ replaced by cos $m\phi$. The dc amplitude is given by

$$A_0 = \frac{1}{2\pi}\int_0^{2\pi} B(\phi)\, d\phi \, .$$

Therefore, given the measured values of the field components, the Fourier analysis can be performed easily to yield the systems of equations to be solved.

Let r_i be the radius of the ith probe location. Let $B_j(r_i,\phi,\cos\theta_i)$ be the component of the magnetic field seen on the jth sensor of the probe at position i. Let $A_0(i,j,\cos\theta_i)$ be the dc amplitude of the components $B_j(r_i,\phi,\cos\theta_i)$. Let $A_1(i,j,\cos\theta_i)$ be the fundamental (i.e., $m = 1$) cosine amplitude of the component $B_j(r_i,\phi,\cos\theta_i)$. Let $A_2(i,j,\cos\theta_i)$ be the fundamental sine amplitude of the component $B_j(r_i,\phi,\cos\theta_i)$. These components are given by the following equations:

$$A_0(i,j,\cos\theta_i) = \frac{1}{2\pi}\int_0^{2\pi} B_j(r_i,\phi,\cos\theta_i)\, d\phi \, , \tag{21a}$$

$$A_1(i,j,\cos\theta_i) = \frac{1}{\pi}\int_0^{2\pi} B_j(r_i,\phi,\cos\theta_i)\cos\phi \, d\phi \, , \tag{21b}$$

and

$$A_2(i,j,\cos\theta_i) = \frac{1}{\pi}\int_0^{\pi} B_j(r_i,\phi,\cos\theta_i)\sin\phi \, d\phi \, . \tag{21c}$$

By use of Equations 18, 19, and 20, these quantities can be related to the various multipole coefficients. For $\theta_i = \pi/2$, the multipole coefficients can be equated as follows:

$$A_1(i,1,0) = \sum_{j=1}^{\infty} \frac{j+1}{r_i^{j+2}} P_j^1(0) a_{j1} \, , \tag{22a}$$

$$A_2(i,2,0) = \sum_{j=1}^{\infty} \frac{1}{r_i^{j+2}} P_j^1(0) a_{j1} \, , \tag{22b}$$

$$A_2(i,1,0) = \sum_{j=1}^{\infty} \frac{j+1}{r_i^{j+2}} P_j^1(0) b_{j1} \, , \tag{22c}$$

$$A_1(i,2,0) = -\sum_{j=1}^{\infty} \frac{1}{r_i^{j+2}} P_j^1(0) b_{j1} \ , \tag{22d}$$

and,

$$A_0(i,3,0) = -\sum_{j=1}^{\infty} \frac{1}{r_i^{j+2}} P_j^1(0) a_{j0} \ .^{*} \tag{22e}$$

For $\theta = 0$,

$$A_1(i,1,1) = -\sum_{j=1}^{\infty} \frac{1}{r_i^{j+2}} \frac{\partial}{\partial\theta} P_j^1(1) a_{j1} \ , \tag{23a}$$

$$A_2(i,2,1) = \sum_{j=1}^{\infty} \frac{1}{r_i^{j+2}} \frac{P_j^1(1)}{\sin 0} a_{j1} \ , \tag{23b}$$

$$A_2(i,1,1) = -\sum_{j=1}^{\infty} \frac{1}{r_i^{j+2}} \frac{\partial}{\partial\theta} P_j^1(1) b_{j1} \ , \tag{23c}$$

$$A_1(i,2,1) = -\sum_{j=1}^{\infty} \frac{1}{r_i^{j+2}} \frac{P_j^1(1)}{\sin 0} b_{j1} \tag{23d}$$

and

$$A_0(i,3,1) = \sum_{j=1}^{\infty} \frac{j+1}{r_i^{j+2}} P_j^0(1) a_{j0} \ . \tag{23e}$$

For $\theta = \pi$,

$$A_1(i,1,-1) = \sum_{j=1}^{\infty} \frac{1}{r_i^{j+2}} \frac{\partial}{\partial\theta} P_j^1(-1) a_{j1} \ , \tag{24a}$$

$$A_2(i,2,-1) = \sum_{j=1}^{\infty} \frac{1}{r_i^{j+2}} \frac{P_j^1(-1)}{\sin \pi} a_{j1} \ , \tag{24b}$$

$$A_2(i,1,-1) = \sum_{j=1}^{\infty} \frac{1}{r_i^{j+2}} \frac{\partial}{\partial\theta} P_j^1(-1) b_{j1} \ , \tag{24c}$$

---

* $\frac{\partial}{\partial\theta} P_j^m \cos\theta = m \cot\theta \, P_j^m \cos\theta - P_j^{m+1} \cos\theta$.

$$A_1(i,2,-1) = -\sum_{j=1}^{\infty} \frac{1}{r_i^{j+2}} \frac{P_j^1(-1)}{\sin \pi} b_{j1} \ , \tag{24d}$$

and

$$A_0(i,3,-1) = -\sum_{j=1}^{\infty} \frac{j+1}{r_i^{j+2}} P_j^0(-1) a_{j0} \ , \tag{24e}$$

It will be shown shortly that the sums in Equation 22 contain only terms for which j is odd, whereas the sums of Equations 23 and 24 contain all values of j. However, the symmetry of the functions P_j^m can be used to construct equations containing only odd values of j. To do this, the radii of the two probes at $\theta = 0$ and $\theta = \pi$ must be identical (let it be r_A). The $P_j^m(x)$ have the following properties:

$$P_j^m(-x) = (-1)^{j+m} P_j^m(x)$$

and

$$\frac{\partial}{\partial \theta} P_j^m(-x) = (-1)^{j+m+1} \frac{\partial}{\partial \theta} P_j^m(x) \ .$$

Consider now the term

$$\begin{aligned} \frac{1}{2}\left[A_1(i,1,1) + A_1(i,1,-1)\right] &= \sum_{j=1}^{\infty} \frac{1}{r_A^{j+2}} a_{j1} \left[-\frac{\partial}{\partial \theta} P_j^1(1) + \frac{\partial}{\partial \theta} P_j^1(-1)\right] \\ &= \sum_{j=1}^{\infty} \frac{1}{r_A^{j+2}} a_{j1} \frac{\partial}{\partial \theta} P_j^1(1)[(-1) + (-1)^{j+2}] \\ &= \sum_{j \text{ odd}} \frac{1}{r_A^{j+2}} \frac{\partial}{\partial \theta} P_j^1(1) a_{j1} \ . \end{aligned}$$

Likewise, all terms of the form

$$\frac{1}{2}\left[A_k(i,j,1) + A_k(i,j,-1)\right]$$

can be equated to sums involving only odd values of j. Notice also that since $P_j^2(\pm 1) = 0$, $\partial P_j^1(+1)/\partial \theta = P_j^1(+1)/\sin 0$ and $\partial P_j^1(-1)/\partial \theta = -P_j^1(-1)/\sin \pi$. Hence,

$$A_1(i,1,k) = -A_2(i,2,k)$$

and

$$A_2(i,1,k) = A_1(i,2,k) \ ,$$

for $k = \pm 1$.

Therefore, some of Equations 23 and 24 are identical. Let us, then, construct three new equations of the same form as those in Equation 22 (i.e., j = odd values only) which contain all the information present in Equations 23 and 24:

$$A_1(A) = \frac{1}{4}\left[A_1(i,1,1) + A_1(i,1,-1) - A_2(i,2,1) - A_2(i,2,-1)\right] , \tag{25a}$$

$$A_2(A) = \frac{1}{4}\left[A_2(i,1,1) + A_2(i,1,-1) + A_1(i,2,1) + A_1(i,2,-1)\right] , \tag{25b}$$

and

$$A_0(A) = \frac{1}{4}\left[A_0(i,3,1) + A_0(i,3,-1)\right] . \tag{25c}$$

These quantities can be equated to the multipole coefficients as follows:

$$-A_1(A) = \sum_{j\ \text{odd}} \frac{1}{r_A^{j+2}} \frac{\partial}{\partial\theta} P_j^1(1) a_{j1} , \tag{26a}$$

$$-A_2(A) = \sum_{j\ \text{odd}} \frac{1}{r_A^{j+2}} \frac{\partial}{\partial\theta} P_j^1(1) b_{j1} , \tag{26b}$$

and

$$+A_0(A) = \sum_{j\ \text{odd}} \frac{1}{r_A^{j+2}} P_j^0(1) a_{j0} . \tag{26c}$$

These equations, along with Equations 22, are the equations that must be solved to determine the dipole moment of the source. They can be placed in a more convenient form if the quantities $P_j^m \cos\theta$ are replaced with their literal form. For example, it is well known that $P_j^0(1) = 1$ for all j. Hence, Equation 26c may be rewritten

$$A_0(A) = \sum_{j\ \text{odd}} \frac{j+1}{r_A^{j+2}} a_{j0} .$$

Similar results can be derived for the other values of the associated Legendre functions from the generating function for the Legendre polynomials. Since this function is

$$F(h,x) = (1 - 2hx + h^2)^{-1/2}$$

$$= \sum_{j=0}^{\infty} h^j P_j(x) ,$$

The quantities $P_j^1(0)$ can now be computed as follows. Consider

$$(1-x^2)^{1/2}\frac{\partial}{\partial x}F(h,x) = \sum_{j=0}^{\infty} h^j (1-x^2)^{1/2}\frac{\partial}{\partial x}P_j(x)$$

$$= \frac{h(1-x^2)^{1/2}}{(1-2hx+h^2)^{3/2}} \quad . \tag{27}$$

From the definition of $P_j^m(x)$

$$P_j^m(x) = (1-x^2)^{m/2}\left(\frac{\partial}{\partial x}\right)^m P_j(x) \, .$$

Equation 27 becomes

$$\sum_{j=1}^{\infty} h^j P_j^1(x) = \frac{h(1-x^2)^{1/2}}{(1-2hx+h^2)^{3/2}} \, .$$

For $\theta = \pi/2$, $x = 0$, we have

$$\sum_{j=0}^{\infty} h^j P_j^1(0) = h(1+h^2)^{3/2} \, . \tag{28}$$

The right-hand side of this equation can now be expanded in a Taylor series. The result is

$$h(1+h^2)^{-3/2} = h\left(1 - \frac{3}{2}h^2 + \frac{3}{2}\cdot\frac{5}{2}\frac{h^4}{2!} - \frac{3}{2}\cdot\frac{5}{2}\cdot\frac{7}{2}\frac{h^6}{3!} + \cdots\right)$$

$$= \sum_{j \text{ odd}} \frac{j!!}{\left(\frac{j-1}{2}\right)!}\left(-\frac{1}{2}\right)^{(j-1)/2} h^j$$

If this is set equal to the left hand side of Equation 28,

$$P_j^1(0) = \left(-\frac{1}{2}\right)^{(j-1)/2}\frac{j!!}{\left(\frac{j-1}{2}\right)!} \qquad \text{for } j \text{ odd},$$

and

$$P_j^1(0) = 0 \, , \qquad \text{for } j \text{ even}.$$

A similar procedure can be followed for $\partial P_j^1(1)/\partial\theta$. The result is

$$\frac{\partial}{\partial\theta}P_j^1(1) = \frac{P_j^1(1)}{\sin 0} = \frac{1}{2}j(j+1) \, .$$

These values can now be substituted into Equations 22 and 26 with the index j replaced by the index $2k - 1$, where $k = 1, 2, 3, \ldots, \infty$. The resulting equations are:

$$A_1(i,1,0) = \sum_{k=1}^{\infty} \left(-\frac{1}{2}\right)^{k-1} \frac{2k(2k-1)!!}{(k-1)!} \frac{1}{r_i^{2k+1}} a_{2k-1,1} \quad , \tag{29a}$$

$$A_2(1,2,0) = \sum_{k=1}^{\infty} \left(-\frac{1}{2}\right)^{k-1} \frac{(2k-1)!!}{(k-1)!} \frac{1}{r_i^{2k+1}} a_{2k-1,1} \quad , \tag{29b}$$

$$-A_1(A) = \sum_{k=1}^{\infty} \frac{k(2k-1)}{r_A^{2k+1}} a_{2k-1,1} \quad , \tag{29c}$$

$$-A_2(i,1,0) = \sum_{k=1}^{\infty} \left(-\frac{1}{2}\right)^{k-1} \frac{2k(2k-1)!!}{(k-1)!} \frac{1}{r_i^{2k+1}} b_{2k-1,1} \quad , \tag{30a}$$

$$-A_1(i,2,0) = \sum_{k=1}^{\infty} \left(-\frac{1}{2}\right)^{k-1} \frac{(2k-1)!!}{(k-1)!} \frac{1}{r_i^{2k+1}} b_{2k-1,1} \quad , \tag{30b}$$

$$-A_2(A) = \sum_{k=1}^{\infty} \frac{k(2k-1)}{r_A^{2k+1}} b_{2k-1,1} \quad , \tag{30c}$$

$$-A_0(i,3,0) = \sum_{k=1}^{\infty} \left(-\frac{1}{2}\right)^{k-1} \frac{(2k-1)!!}{(k-1)!} \frac{1}{r_i^{2k+1}} a_{2k-1,0} \quad , \tag{31a}$$

and

$$A_0(A) = \sum_{k=1}^{\infty} \frac{2k}{r_A^{2k+1}} a_{2k-1,0} \quad . \tag{31b}$$

Assume now that the magnetic field is measured by N_p different magnetometer probes. This means that the number of equations in each of the above sets is fixed. Since each of these equations contains, in theory, an infinite number of terms, no unique solution is possible. One must therefore make the assumption that each of these series can be approximated by a finite number of terms. This seems reasonable, since the sums are power series in $r^{-(2k+1)}$. The higher terms can therefore be expected to contribute increasingly smaller amounts to the series.

Specifically, in order to obtain a unique solution, the number of unknowns must be less than or equal to the number of equations. Since the lower order terms are expected to be larger than the higher order terms, it seems logical to truncate the series rather than to select the various terms to be included by some procedure.

The number of equations one is able to construct for a given number N_p of probes depends upon how these probes are deployed. There are basically two configurations that can be considered. One is formed by placing all the sensors in the horizontal plane. In this case (known as the + 1 configuration), there are $2N_p$ equations for the X- and Y-axis moments and N_p equations for the Z-axis moments. The other configuration (known as the 0 configuration) employs two of the sensors above and below the source (i.e., along the Z axis). Here, there are $2N_p - 3$ equations for the X- and Y-axis moments and $N_p - 1$ equations for the Z-axis moments. No matter which configuration is used, each equation in a set is of the form

$$y_i = \sum_{j=1}^{M} c_{ij} q_j \ , \tag{32}$$

where y_i is a Fourier coefficient, c_{ij} is a known coefficient, and q_j is an unknown quantity proportional to the ith multipole moment coefficient.

Solution of the Near-Field Equations

The problem now is to determine the set of coefficients that best satisfy Equations 32. The criterion for "best" that will be used here is a least squares one; that is, the multipole coefficients will be chosen to minimize the sum of the squares of the deviations of the calculated Fourier coefficients from the "measured" ones.

It is now necessary to define several quantities that will be used in the following discussion. Let $f(y)$ be the probability that if one observes a quantity, that observation will yield the value y for that quantity. Usually, the values of y form a continuous set. Then $f(y)$ is defined so that $f(y)\,dy$ is the probability that an observation lies in a range dy centered at y. The expectation value of a function $q(y)$ is defined as

$$< q > = \int q(y) f(y)\, dy \ ,$$

where the integration extends over all the possible values of y (the integration becomes a summation if the allowed values of y are discrete). The population mean, or true value Y of y, is defined as

$$Y = < y >$$

for a very large number of observations.

The variance of a quantity is defined as the average of the squares of the deviations from the true value. Hence,

$$\text{var}\, y = < (y - Y)^2 > .$$

The covariance of two quantities y and z is defined as

$$\text{cov}\,(y,z) = \langle (y - Y)(z - Z) \rangle$$

$$= \int (y - Y)(z - Z) f(y,z)\, dy\, dz\ ,$$

where $f(y,z)\, dy\, dz$ is the probability that the observations of y and z lie simultaneously in the range dy about y and dz about z.

In most cases, the probability function $f(y)$ is not known. Also, the number of measurements available is usually small. Therefore one must estimate the true values of the measured quantities by some method. An unbiased estimate is one whose expectation value is the true value of the quantity. Hence, the population mean can be estimated as an average value given by

$$\bar{y} = \frac{1}{N} \sum_{i=1}^{N} y_i\ .$$

Also, the standard deviation of an observation can be estimated from the deviations from the mean v_i:

$$v_i = y_i - \bar{y}$$

$$\langle v_i^2 \rangle = \left\langle \left[y_i - Y - \frac{1}{N} \sum_{i=1}^{N} (y_i - Y) \right]^2 \right\rangle$$

$$= \frac{N - 1}{N} \text{var}\, y\ .$$

Hence,

$$\left\langle \sum_{i=1}^{N} v_i^2 \right\rangle = (N - 1)\, \text{var}\, y = (N - 1)\sigma^2\ .$$

One therefore estimates the variance σ^2 of the observations by the quantity S^2 given by

$$S^2 = \frac{\sum_{i=1}^{N} (y_i - \bar{y})^2}{N - 1}\ .$$

The variance of the mean is given by

$$\text{var}\, \bar{y} = \frac{\text{var}\, y}{N}\ .$$

Hence,

$$S^2(\bar{y}) = \frac{\sum_{i=1}^{N} (y_i - \bar{y})^2}{N(N-1)}$$

will provide an estimate of the variance of the mean.

The above discussion can now be extended to more than one variable. Let y_i denote the average of a large number of measurements of a variable. Let σ_i be the standard deviation associated with y_i. A relationship of the form

$$y_i = \sum_{j=1}^{M} c_{ij} q_j \tag{33}$$

is assumed to exist between the y_i and the unknown coefficients q_j. The best q_j values in a least squares sense are needed, along with their associated variances. Assume that there are N known y_i. Let us call the right-hand side of Equation 33 the theoretical expression for y_i and denote its value (for a given set of q_j) by c_i.

The least squares postulate states that the best coefficients minimize the mean of the squares of deviations from the means y_i. In symbols,

$$\sum_{i=1}^{N} (y_i - c_i)^2$$

should be minimized. However, the scatter of observations about each of the N points is different (σ_i^2 being a measure of this scatter). Therefore, the deviations should be weighted by dividing by σ_i^2. The least squares principle then makes

$$\sum_{i=1}^{N} \frac{(y_i - c_i)^2}{\sigma_i^2} = \frac{1}{\sigma^2} \sum_{i=1}^{N} w_i (y_i - c_i)^2 \tag{34}$$

a minimum, with $w_i = \sigma^2 / \sigma_i^2$ and σ^2 = a constant.

Differentiating Equation 34 with respect to the q_j and equating the results to zero yields the M so-called normal equations of the system. These can easily be shown to be

$$\sum_{i=1}^{N} w_i y_i c_{ik} - \sum_{j=1}^{M} \left(\sum_{i=1}^{N} w_i c_{ij} c_{ik} \right) q_j = 0 . \tag{35}$$

These equations can be written in standard matrix notation as

$$D_k = \sum_{j=1}^{M} G_{kj} q_j \ , \tag{36}$$

where the substitutions are obvious from the previous discussion. One method of solution is direct inversion of the matrix G. If this inverse is ϕ,

$$\sum_{k=1}^{M} \phi_{rk} D_k = \sum_{k=1}^{M} \sum_{j=1}^{M} \phi_{rk} G_{kj} q_j$$

$$= \sum_{j=1}^{M} \delta_{rj} q_j$$

$$= q_r \ .$$

Hence, the equations are solved, and the quantities q_j, given by

$$q_j = \sum_{k=1}^{M} \phi_{jk} \sum_{i=1}^{N} w_i c_{ik} y_i \ , \tag{37}$$

provide unbiased estimates of the true coefficients $\overline{q}_j$.

The variance of these quantities is easily determined, since they are linear functions of the y_i:

$$\sigma^2(q_j) = \sum_{i=1}^{N} (\partial q_j / \partial y_i)^2 \sigma_i^2$$

$$= \sum_{i=1}^{N} \left(\sum_{k=1}^{M} \phi_{jk} w_i c_{ik} \right) \left(\sum_{r=1}^{M} \phi_{jr} w_i c_{ir} \right) \sigma_i^2$$

$$= \sum_{k=1}^{M} \sum_{r=1}^{M} \phi_{jk} \phi_{jr} \left(\sum_{i=1}^{N} w_i c_{ik} c_{ir} \right) \sigma^2$$

$$= \sum_{k=1}^{M} \sum_{r=1}^{M} \phi_{jk} \phi_{jr} G_{kr} \sigma^2$$

$$= \sum_{k=1}^{M} \phi_{jk} \delta_{jk} \sigma^2$$

$$= \phi_{jj} \sigma^2 \ .$$

The expression for σ^2 can now be estimated from the residuals as follows: Consider

$$v_i = y_i - \sum_{j=1}^{M} c_{ij} q_j \ .$$

Since

$$\langle v_i \rangle = 0 \ ,$$

we can write

$$\begin{aligned} \langle (v_i - \bar{v}_i)^2 \rangle &= \langle v_i^2 \rangle \\ &= \text{var } v_i \\ &= \text{var } y_i - 2 \sum_{j=1}^{M} w_i c_{ij} \text{ cov } (y_i, q_j) + \sum_{j=1}^{M} \sum_{k=1}^{M} w_i^2 c_{ij} c_{ik} \text{ cov } (q_j, q_k) \ . \end{aligned}$$

Now

$$\text{var } y_i = \sigma_i^2 \ ,$$

and

$$\begin{aligned} \text{cov } (q_j, q_k) &= \langle (q_j - \bar{q}_j)(q_k - \bar{q}_k) \rangle \\ &= \left\langle \sum_{i=1}^{M} \sum_{r=1}^{N} \phi_{ki} w_r c_{ri} (y_r - Y_r) \sum_{p=1}^{M} \sum_{s=1}^{N} \phi_{jp} w_s c_{sp} (y_s - Y_s) \right\rangle \\ &= \sum_{i=1}^{M} \sum_{p=1}^{M} \sum_{r=1}^{N} \sum_{s=1}^{N} \phi_{ki} \phi_{jp} w_r w_s c_{ri} c_{sp} \langle (y_r - Y_r)(y_s - Y_s) \rangle \ . \end{aligned}$$

Now

$$\langle (y_r - Y_r)(y_s - Y_s) \rangle = \delta_{rs} \sigma_s^2 \ .$$

Hence,

$$\text{cov } (q_j, q_k) = \sum_{i=1}^{M} \sum_{r=1}^{M} \sum_{s=1}^{N} \phi_{ki} \phi_{jr} c_{sr} c_{sk} w_s^2 \sigma_s^2 \ ,$$

but

$$w_s = \sigma^2 / \sigma_s^2 \ .$$

Therefore,

$$\operatorname{cov}(q_j, q_k) = \sum_{i=1}^{M} \sum_{r=1}^{M} \phi_{ki}\phi_{jr} \sum_{s=1}^{N} w_s c_{sr} c_{sk} \sigma^2$$

$$= \sum_{i=1}^{M} \phi_{ki}\delta_{jk}\sigma^2$$

$$= \phi_{jk}\sigma^2 \ .$$

Also,

$$\operatorname{cov}(y_i, q_j) = \left\langle (y_i - Y_i)(q_j - \bar{q}_j) \right\rangle$$

$$= \sum_{k=1}^{M} \sum_{s=1}^{N} \phi_{jk} c_{sk} w_s \left\langle (y_i - Y_i)(y_s - Y_s) \right\rangle$$

$$= \sum_{k=1}^{M} \phi_{jk} c_{ik} \sigma^2 \ .$$

Hence,

$$\operatorname{var} v_i = \sigma_i^2 + \sum_{k=1}^{M} \sum_{j=1}^{M} c_{ij} c_{ik} \phi_{jk} \sigma^2 - 2 \sum_{j=1}^{M} \sum_{k=1}^{M} c_{ij} \phi_{jk} c_{ik} \sigma^2$$

$$= \sigma_i^2 - \sum_{j=1}^{M} \sum_{k=1}^{M} \phi_{jk} c_{ij} c_{ik} \sigma^2 \ .$$

Now

$$\left\langle \sum_{i=1}^{N} w_i v_i^2 \right\rangle = \sum_{i=1}^{N} w_i \operatorname{var} v_i$$

$$= \sum_{i=1}^{N} w_i \sigma_i^2 - \sum_{j=1}^{M} \sum_{k=1}^{M} \phi_{jk} \left(\sum_{i=1}^{N} w_i c_{ij} c_{ik} \right) \sigma^2$$

$$= N\sigma^2 - \sum_{j=1}^{M} \delta_{jk} \sigma^2$$

$$= (N - M)\sigma^2 \ .$$

Hence, σ^2 can be estimated as the quantity S^2 given by

$$S^2 = \frac{\sum_{i=1}^{N} w_i v_i^2}{N - M} \quad .$$

Also, the variance of q_j is estimated as

$$S^2(q_j) = \phi_{jj} s^2$$

$$= \frac{\phi_{jj}}{N - M} \sum_{i=1}^{N} w_i v_i^2 \quad . \tag{38}$$

A Statistical Test

Thus far it has tacitly been assumed that any errors in the y_i were due to the net effect of a number of small disturbances. In this case, the errors will be distributed about the population mean according to the so-called "normal distribution" of statistical theory. This means that the probability of obtaining a value y_i will be proportional to

$$\exp\left[-\left(\frac{y_i - Y_i}{\partial \sigma_i}\right)^2\right] dy_i \ ,$$

where Y_i is the population mean.

If x is a linear function of the y_i (e.g., a multipole coefficient), X the "true" value of this function (corresponding to the Y_i), and $S(x)$ the estimated standard deviation of x based on the estimate

$$S^2 = \sum_{i=1}^{N} w_i v_i / \nu$$

of σ^2, then it can be shown that the variable

$$t = (x - X)/S(x) \tag{39}$$

is distributed according to the function

$$f(t)\,dt = \frac{\Gamma\left(\frac{1}{2}\nu + \frac{1}{2}\right)}{\Gamma\left(\frac{1}{2}\nu\right)\sqrt{\pi\nu}} \left(1 + \frac{t^2}{\nu}\right)^{-(1/2)(\nu+1)} dt \ .$$

This is often referred to as Student's distribution, and tables of the variable t can be used to test the significance of the departure from an assumed true value. In particular, it can be used to construct confidence intervals for the value x. For example, for a given number of degrees of freedom ν, the probability that $|t| \geq t_a$ can be determined from various tables. Let this probability be a. Therefore, it can

be said that the probability that the deviation from the population mean is greater than $t_a s(x)$ in magnitude is a for a given experiment.

This discussion has provided a method by which the various multipole coefficients and their associated uncertainties can be estimated. This method is based upon one basic assumption: The infinite multipole expansion for the Fourier coefficients can be truncated without introducing significant errors. The logical question to ask now is what happens if the fundamental assumption is invalid? That is, what happens in the case when one or more of the multipole coefficients, which were assumed negligible, actually contributes a significant amount to the Fourier coefficients? The answer is that the q_j will no longer be good estimates of the actual multipole moment coefficients n_j. This is apparent from the actual expression for the y_i:

$$y_i = \sum_{j=1}^{\infty} c_{ij} n_j$$

$$= \sum_{j=1}^{M} c_{ij} n_j + \sum_{j=m+1}^{\infty} c_{ij} n_j$$

$$= \sum_{j=1}^{M} c_{ij} n_j + \delta_i \, .$$

The q_j can be calculated from Equation 37:

$$q_j = \sum_{k=1}^{M} \phi_{jk} \sum_{i=1}^{N} w_i c_{ik} \left(\sum_{r=1}^{M} c_{ir} n_r + \delta_i \right)$$

$$= n_j + \sum_{k=1}^{M} \sum_{i=1}^{N} w_i c_{ik} \phi_{jk} \delta_i$$

$$= n_j + e_j \, .$$

If the basic assumption is untrue, systematic errors can be expected in the q_j which cannot be eliminated by the above analysis. One can expect the errors e_j to change as the order of fit M of the system is changed. Specifically, e_j can be written as a sum over the multipole coefficients from $M + 1$ to ∞. Hence, as the value of M increases, more of the coefficients are eliminated, and the error might be expected to decrease somewhat. However, this behavior is not definite, and since the error e_j cannot be separated from the m_j, another procedure must be found by which the accuracy of the q_j can be estimated.

CHAPTER IV

ERROR ANALYSIS

Introduction

Consider, for a moment, the currents and magnetic material within the spacecraft. The currents are macroscopic currents flowing through coils which permeate the source. Given currents of this type, a magnetization density which will produce an identical magnetic field outside the source can, in principle, be determined. This magnetization density will not vary appreciably over small distances. This is also the case with the magnetization of the magnetic material. The spacecraft source can therefore be divided into macroscopic subvolumes whose magnetizations are fairly uniform. Each of these subvolumes can be considered to contain a point dipole source whose magnitude and direction are determined by the average magnetization density in that subvolume. By adjusting the size of each subvolume, the magnetic field of this ensemble of point dipoles can be made to coincide with that of the actual spacecraft to any desired degree of accuracy.

Actually, a procedure such as this would be impossible; but the point is clear: The spacecraft can be represented by a finite number of point dipole sources, and its field can be written as the sum over a finite number of these point dipole fields. It would, therefore, seem that the determination of the dipole moment of a point dipole source is of fundamental importance, and that the errors that arise in this case are definitely related to those of the general case.

Let $\mathbf{m}(\mathbf{k})$ be the moment of a point dipole located at the point P specified by the position vector $\mathbf{k}$. Let the field produced by this dipole be measured by N_p probes in either the +1 or the 0 configuration, as in Figure 2. The magnetization density $\mathbf{M}(\mathbf{r})$ which describes this source is representable by

$$\mathbf{M}(\mathbf{r}) = \mathbf{m}(\mathbf{k})\delta(\mathbf{r} - \mathbf{k}) .$$

This magnetization will give rise to the multipole coefficients of the system as given in Equations 16. Upon integration by parts, it will be found that integrals of the form

$$\int_{\text{volume}} f(\mathbf{r})\nabla \cdot \mathbf{g}(\mathbf{r})\, dV$$

may be written as

$$-\int_{\text{volume}} \mathbf{g}(\mathbf{r}) \cdot \nabla f(r)\, dV .$$

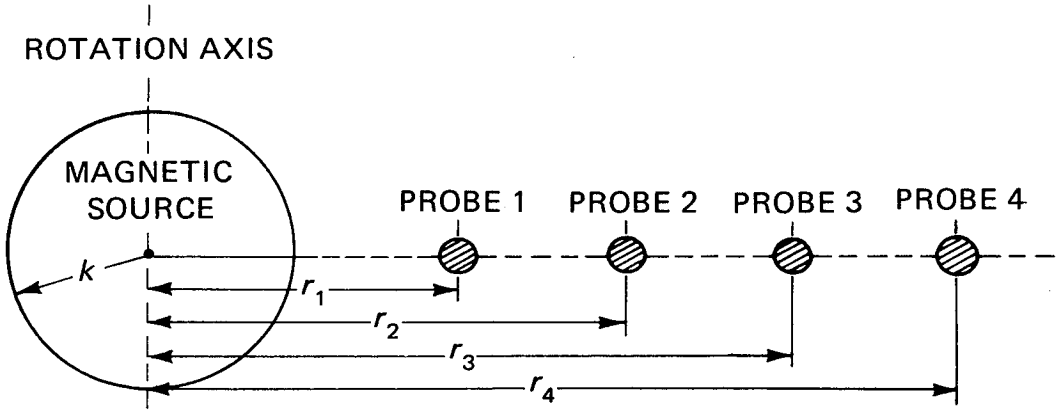

(a) + 1 configuration.

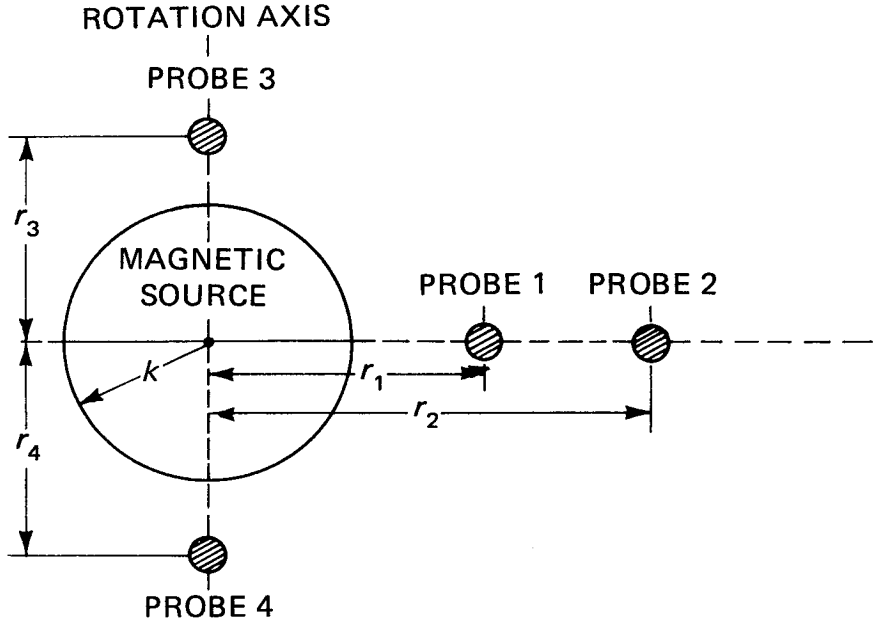

(b) Zero configuration.

Figure 2—Probe configurations for typical test situations ($S_p = 2k/r_1$ and $r_{1j} = r_1/r_j$).

Hence, $a_{jm}(\mathbf{k})$ is

$$a_{jm}(\mathbf{k}) = (2 - \delta_{j0}) \frac{(j-m)!}{(j+m)!} \int \mathbf{m}(\mathbf{k}) \delta(\mathbf{r} - \mathbf{k}) \cdot \nabla rj P_j^m(\cos\theta) \cos m\phi \, d^3\mathbf{r}$$

$$= (2 - \delta_{j0}) \frac{(j-m)!}{(j+m)!} \mathbf{m}(\mathbf{k}) \cdot \nabla rj P_j^m(\cos\theta) \sin m\phi \Big|_{\mathbf{r}=\mathbf{k}} . \tag{40}$$

Similarly, for $b_{jm}(\mathbf{k})$,

$$b_{jm}(\mathbf{k}) = 2 \frac{(j-m)!}{(j+m)!} \mathbf{m}(\mathbf{k}) \cdot \nabla rj P_j^m(\cos\theta) \cos m\phi \Big|_{\mathbf{r}=\mathbf{k}} . \tag{41}$$

The only coefficients of interest in this case are those for which $m = 0$, 1 and j = odd. Therefore, define

$$n_j(1,\mathbf{k}) = a_{2j-1,1}(\mathbf{k}) , \tag{42a}$$

$$n_j(2,\mathbf{k}) = b_{2j-1,1}(\mathbf{k}) , \tag{42b}$$

and

$$n_j(3,\mathbf{k}) = a_{2j-1,0}(\mathbf{k}) , \tag{42c}$$

which one can write as

$$n_j(s,\mathbf{k}) = \mathbf{m}(\mathbf{k}) \cdot \mathbf{h}_j(s,\mathbf{k}) .$$

As before, the actual Fourier coefficients for the sth axis can be written as

$$y_i(s,\mathbf{k}) = \sum_{j=1}^{\infty} c_{ij}(s) n_j(s,\mathbf{k}) .$$

Now, the least squares coefficients $q_r(s,k)$ can be determined as before from Equation 37:

$$q_r(s,\mathbf{k}) = \sum_{p=1}^{M(s)} \phi_{rp}(s) \sum_{i=1}^{N(s)} c_{ip}(s) w_i(s) y_i(s,\mathbf{k})$$

$$= \sum_{j=1}^{\infty} \sum_{p=1}^{M(s)} \sum_{i=1}^{N(s)} \phi_{rp}(s) c_{ip}(s) w_i(s) c_{ij}(s) n_j(s,\mathbf{k})$$

$$= n_r(s,\mathbf{k}) + \sum_{j=M(s)+1}^{\infty} \sum_{p=1}^{M(s)} \sum_{i=1}^{N(s)} \phi_{rp}(s) w_i(s) c_{ip}(s) c_{ij}(s) n_j(s,\mathbf{k})$$

$$= n_r(s,\mathbf{k}) + \mathbf{m}(\mathbf{k}) \cdot \left[\sum_{j=M(s)+1}^{\infty} \sum_{p=1}^{M(s)} \sum_{i=1}^{N(s)} \phi_{rp}(s) w_i(s) c_{ip}(s) c_{ij}(s) \mathbf{h}_j(s,\mathbf{k}) \right]$$

$$= n_r(s,\mathbf{k}) + \mathbf{m}(\mathbf{k}) \cdot \mathbf{Q}_r(s,\mathbf{k}) \,. \tag{43}$$

Hence, the error in the coefficient $q_r(s,\mathbf{k})$ is represented by the term $\mathbf{m}(\mathbf{k}) \cdot \mathbf{Q}_r(s,\mathbf{k})$.

Consider now an assembly of point dipoles. The results can be written immediately from a summation over all vectors $\mathbf{k}$. Therefore, the least squares coefficient $q_r(s)$ is given by

$$q_r(s) = \sum_{\mathbf{k}} q_r(s,\mathbf{k})$$

$$= \sum_{\mathbf{k}} n_r(s,\mathbf{k}) + \sum_{\mathbf{k}} \mathbf{m}(\mathbf{k}) \cdot \mathbf{Q}_r(s,\mathbf{k})$$

$$= n_r(s) + \sum_{\mathbf{k}} \mathbf{m}(\mathbf{k}) \cdot \mathbf{Q}_r(s,\mathbf{k})$$

$$= n_r(s) + e_r(s) \,,$$

where

$$e_r(s) = \sum_{\mathbf{k}} \mathbf{m}(\mathbf{k}) \cdot \mathbf{Q}_r(s,\mathbf{k}) \,,$$

if $\mathbf{m}(\mathbf{k})$ is discrete, or

$$e_r(s) = \int \mathbf{m}(\mathbf{k}) \cdot \mathbf{Q}_r(s,\mathbf{k}) \, d^3\mathbf{k} \,,$$

if $\mathbf{m}(\mathbf{k})$ is a continuous function of the vector $\mathbf{k}$. Now if one could say

$$q_r(s) = n_r(s) \pm \delta \,,$$

where the magnitude of δ were known, one would know the limits within which $n_r(s)$ must lie.

Consider therefore $|e_r(s)|$ such that

$$|e_r(s)| = \left| \int \mathbf{m}(\mathbf{k}) \cdot \mathbf{Q}_r(s,\mathbf{k}) \, d^3\mathbf{k} \right|$$

$$\leqslant \int |\mathbf{m}(\mathbf{k}) \cdot \mathbf{Q}_r(s,\mathbf{k})| \, d^3\mathbf{k}$$

$$\leqslant \int |\mathbf{m}(\mathbf{k})|\,|\mathbf{Q}_r(s,\mathbf{k})|\,d^3\mathbf{k}$$

$$\leqslant Q_r^m(s,\mathbf{k}) \int |\mathbf{m}(\mathbf{k})|\,d^3\mathbf{k}\,,$$

where $Q_r^m(s,k)$ is the maximum value of the magnitude of $\mathbf{Q}_r(s,\mathbf{k})$ for any vector $\mathbf{k}$ (within the confines of the source). Similarly, for discrete values of $\mathbf{m}(\mathbf{k})$

$$|e_r(s)| \leqslant Q_r^m(s,\mathbf{k}) \sum_{\mathbf{k}} |\mathbf{m}(\mathbf{k})|\,.$$

Now, the vector $\mathbf{Q}_r(s,\mathbf{k})$ and the quantity $Q_r^m(s,k)$ are independent of the source in question. Assume for now that they can be determined by some procedure and hence are known. The error is related to the particular source through the terms

$$\int |\mathbf{m}(\mathbf{k})|\,d^3k \text{ or } \sum_{\mathbf{k}} |\mathbf{m}(\mathbf{k})|\,.$$

This quantity represents the magnitude of the maximum possible dipole moment of that particular source. It is, in general, impossible to calculate. Therefore, some method of estimation must be devised.

The magnitude of this term is dependent upon the magnetic components within the source. If they are weak, the term will be small. If they are strong, the term will be large. Such is the case with the magnetic field of the object. If the components are weak, the field will be small; if they are strong, the field will be large, independent of what the dipole moment is. Also, in the case where

$$\left|\int \mathbf{m}(\mathbf{k})\,d^3\mathbf{k}\right| \doteq \int |\mathbf{m}(\mathbf{k})|\,d^3\mathbf{k}\,,$$

the dipole moment will usually be large compared with the other moments. Hence, as a fairly good approximation,

$$\left|\int \mathbf{m}(\mathbf{k})\,d^3\mathbf{k}\right| = \left[\frac{1}{4}\left(\frac{B_{1pp}}{2} + B_{2pp}\right)^2 + B_{3p}^2\right]^{1/2} r_f^3 = B_e\,, \tag{44}$$

where B_{jpp} is the maximum field excursion seen on the jth sensor of the most distant probe during a rotation, B_{jp} is the maximum value of the field seen on the jth sensor of this probe, and r_f is the radius of this probe. In the cases where the dipole moment is small, the right-hand side of Equation 44 will still be a quantity which will give a measure of the magnitude of the field of the source. The assumption will therefore be made that

$$\int |\mathbf{m}(\mathbf{k})|\,d^3\mathbf{k} = B_e \tag{45}$$

in all cases. This assumption is not really critical as long as the estimate of $e_r(s)$ is not so large that it is useless, or so small that it is unrealistic. Still, it is an assumption whose validity must be tested further. The discussion of this assumption will be deferred until later.

Single-Dipole Error Functions

The form of $\mathbf{Q}_r(s,\mathbf{k})$ must now be examined. Evaluate the quantities $n_j(s,\mathbf{k})$; using Equations 40, 41, and 42, and the Cartesian components of the operator ∇ in the spherical polar coordinate system, write the n_j as

$$n_j(1,\mathbf{k}) = m_1 [S_{1j}(\mathbf{k}) \cos^2 \phi_k + S_{2j}(\mathbf{k}) \sin^2 \phi_k]$$
$$+ m_2 [S_{1j}(\mathbf{k}) - S_{2j}(\mathbf{k})] \cos \phi_k \sin \phi_k + m_3 S_{3j}(\mathbf{k}) \cos \phi_k ,$$
$$n_j(2,\mathbf{k}) = m_1 [S_{1j}(\mathbf{k}) - S_{2j}(\mathbf{k})] \cos \phi_k \sin \phi_k$$
$$+ m_2 [S_{1j}(\mathbf{k}) \sin^2 \phi_k + S_{2j}(\mathbf{k}) \cos^2 \phi_k] + m_3 S_{3j}(\mathbf{k}) \sin \phi_k ,$$

and

$$n_j(3,\mathbf{k}) = m_1 S_{4j}(\mathbf{k}) \cos \phi_k + m_2 S_{4j}(\mathbf{k}) \sin \phi_k + m_3 S_{5j}(\mathbf{k}) ,$$

where m_j = the jth component of $\mathbf{m}(\mathbf{k})$ and

$$S_{1j}(\mathbf{k}) = \frac{k^{2j-2}}{j} \left[\sin \theta_k \, P^1_{2j-1}(\cos \theta_k) + \frac{\cos \theta_k}{2j-1} \frac{\partial}{\partial \theta} P^1_{2j-1}(\cos \theta_k) \right] ,$$

$$S_{2j}(\mathbf{k}) = \frac{k^{2j-2}}{j(2j-1)} \left[\frac{P^1_{2j-1}(\cos \theta_k)}{\sin \theta_k} \right] ,$$

$$S_{3j}(\mathbf{k}) = \frac{k^{2j-2}}{j} \left[\cos \theta_k \, P^1_{2j-1}(\cos \theta_k) - \frac{\sin \theta_k}{2j-1} \frac{\partial}{\partial \theta} P^1_{2j-1}(\cos \theta_k) \right] ,$$

$$S_{4j}(\mathbf{k}) = k^{2j-2} [(2j-1) \sin \theta_k \, P_{2j-1}(\cos \theta_k) - \cos \theta_k \, P^1_{2j-1}(\cos \theta_k)] ,$$

and

$$S_{5j}(\mathbf{k}) = k^{2j-2} [(2j-1) \cos \theta_k \, P_{2j-1}(\cos \theta_k) + \sin \theta_k \, P^1_{2j-1}(\cos \theta_k)] .$$

The quantity $e_{rj}(s)$ is now defined as

$$e_{rj}(s) = \sum_{p=1}^{M(s)} \sum_{i=1}^{N(s)} \phi_{rp}(s) w_i(s) c_{ip}(s) c_{ij}(s) .$$

The quantities $\mathbf{m(k)} \cdot \mathbf{Q}_r(s, \mathbf{k})$ can then be written as

$$\mathbf{m(k)} \cdot \mathbf{Q}_r(1,\mathbf{k}) = m_1 [E_{1r}(1,\mathbf{k}) \cos^2 \phi_k + E_{2r}(1,\mathbf{k}) \sin^2 \phi_k]$$
$$+ m_2 [E_{1r}(1,\mathbf{k}) - E_{2r}(1,\mathbf{k})] \cos \phi_k \sin \phi_k + m_3 E_{3r}(1,\mathbf{k}) \cos \phi_k \ , \quad (46a)$$

$$\mathbf{m(k)} \cdot \mathbf{Q}_r(2,\mathbf{k}) = m_1 [E_{1r}(2,\mathbf{k}) - E_{2r}(2,\mathbf{k})] \cos \phi_k \sin \phi_k$$
$$+ m_2 [E_{1r}(2,\mathbf{k}) \sin^2 \phi_k + E_{2r}(2,\mathbf{k}) \cos^2 \phi_k] + m_3 E_{3r}(2,\mathbf{k}) \sin \phi_k \ , \quad (46b)$$

and

$$\mathbf{m(k)} \cdot \mathbf{Q}_r(3,\mathbf{k}) = m_1 E_{4r}(3,\mathbf{k}) \cos \phi_k + m_2 E_{4r}(3,\mathbf{k}) \sin \phi_k + m_3 E_{5r}(3,\mathbf{k}) \ . \quad (46c)$$

where

$$E_{ir}(s, \mathbf{k}) = \sum_{j=M(s)+1}^{\infty} e_{rj}(s) S_{ij}(\mathbf{k}) \ .$$

Examination of Equations 29 and 30 reveals that the near-field equations for the x and y axes are identical in form. Hence, if the weights w_j in Equation 34 are the same for each axis (which they will be), $e_{rj}(1) = e_{rj}(2)$ for all r and j. Also, since only the errors in the dipole components are of interest, all the $E_{jr}(s, k)$ for which $r \neq 1$ can be neglected. The dipole errors $\mathbf{m(k)} \cdot \mathbf{Q}_1(s, \mathbf{k})$ can now be written in terms of only five error functions. These functions are defined as follows:

$$E_j(\mathbf{k}) = E_{j1}(1,\mathbf{k}) = E_{j1}(2,\mathbf{k}) \ , \quad \text{for } j = 1, 2, 3;$$

and

$$E_j(\mathbf{k}) = E_{j1}(3,\mathbf{k}) \ , \qquad \text{for } j = 4, 5 \ .$$

The value of the function $\mathbf{Q}_1(s, \mathbf{k})$ may be determined for any values of k and θ_k by analyzing suitably chosen single-dipole sources. For example, let the source consist of dipole whose moment is m (components m_1, m_2, and m_3) located at the point $\mathbf{k} = (k, \theta_k ; \phi_k = 0)$. Three determinations of the least squares dipole-moment components (for three different sets of the m_1, m_2, and m_3) on each axis are necessary for a complete definition of the vector $\mathbf{Q}_1(s, \mathbf{k})$ for a particular probe configuration and least squares fit. Hence, if $m_1 = 0$, $m_2 = m_3 = 0$, Equations 43 and 46 give

$$q_1(1) = m_1 + m_1 E_1(\mathbf{k}) \ ,$$

$$q_1(2) = 0 \ ,$$

and

$$q_1(3) = m_1 E_4(\mathbf{k}) \ .$$

Similarly, if $m_2 \neq 0$, $m_1 = m_2 = 0$,

$$q_1(1) = q_1(3) = 0$$

and

$$q_1(2) = m_2 + m_2 E_2(\mathbf{k}) .$$

Also, for $m_3 \neq 0, m_1 = m_2 = 0$,

$$q_1(1) = m_3 E_3(\mathbf{k}) ,$$

$$q_1(2) = 0 ,$$

and

$$q_1(3) = m_3 + m_3 E_5(\mathbf{k}) .$$

Hence, the value of $\mathbf{Q}_1(s, \mathbf{k})$ is known for the vector $\mathbf{k}$. Since the ϕ_k-dependence of the function is known, $\mathbf{Q}_1(s, \mathbf{k})$ is really known on a circle of latitude specified by the angle θ_k on a sphere whose radius is k. In principle, therefore, the vector $\mathbf{Q}_1(s, \mathbf{k})$ can be completely determined if this procedure is repeated for all values of $\mathbf{k}$.

Having done this, one must compute

$$\left|\mathbf{Q}_1(s, \mathbf{k})\right|^2 = \mathbf{Q}_1(s, \mathbf{k}) \cdot \mathbf{Q}_1(s, \mathbf{k}) .$$

from Equations 46:

$$\left|\mathbf{Q}_1(1,\mathbf{k})\right|^2 = \left\{ [E_1(\mathbf{k})]^2 + [E_3(\mathbf{k})]^2 \right\} \cos^2 \phi_k + [E_2(\mathbf{k})]^2 \sin^2 \phi_k ,$$

$$\left|\mathbf{Q}_1(2,\mathbf{k})\right|^2 = \left\{ [E_1(\mathbf{k})]^2 + [E_3(\mathbf{k})]^2 \right\} \sin^2 \phi_k + [E_2(\mathbf{k})]^2 \cos^2 \phi_k ,$$

$$\left|\mathbf{Q}_1(3,\mathbf{k})\right|^2 = [E_4(\mathbf{k})]^2 + [E_5(\mathbf{k})]^2 .$$

Clearly,

$$[Q_1^M(1,\mathbf{k})]^2 \leqslant \left\{ [E_1(\mathbf{k})]^2 + [E_3(\mathbf{k})]^2 \right\}_{\max} + [E_2(\mathbf{k})]^2_{\max} = Q^1 ,$$

$$[Q_1^M(2,\mathbf{k})]^2 \leqslant \left\{ [E_1(\mathbf{k})]^2 + [E_3(\mathbf{k})]^2 \right\}_{\max} + [E_2(\mathbf{k})]^2_{\max} = Q^1 ,$$

$$[Q_1^M(3,\mathbf{k})]^2 \leqslant \left\{ [E_4(\mathbf{k})]^2 + [E_5(\mathbf{k})]^2 \right\}_{\max} = Q^3 .$$

Therefore, the possible systematic errors $|e_1(s)|$ in the dipole components can be estimated from the expression in Equation 45 for $\int |\mathbf{m}(\mathbf{k})| \, d^3k$. Hence, for an estimate of $|e_1(s)|$,

$$|e_1(1)| = |e_1(2)| = Q^1(\mathbf{k}) B_e \tag{47a}$$

and

$$|e_1(3)| = Q^3(\mathbf{k}) B_e . \tag{47b}$$

In summary, then, the procedure for dipole-moment determination should proceed as follows: Specify a given number N_p of magnetometer probes deployed in either the zero or the +1 configuration about the magnetic source. Then, rotate the source through 360 deg to obtain the three components of the magnetic field at each probe location. Now, Equations 21 will give the appropriate Fourier coefficients. If the zero configuration is used, the values of $A_1(A)$, $A_2(A)$, and $A_0(A)$ must be calculated from Equations 25. The next step is to solve for the dipole-moment components axis by axis. For each axis, first determine the order of fit $M(s)$ desired, and then set up the appropriate near-field equations to be solved (Equations 29, 30, and 31).

The least squares analysis now proceeds with the formation for each axis of the matrices D and G, as defined in Equations 35 and 36. For the weights w_i, $1/\sigma_i^2$ must be used, where σ_i is the uncertainty in the measurement of the values of the magnetic field used to calculate the Fourier coefficient Y_i.*

The next step is to invert the G matrix and determine the least squares dipole-moment coefficient $q_1(s)$ from Equation 37, and its associated uncertainty $S^2[q_1(s)]$ from Equation 38. Confidence limits on the value of $q_1(s)$ can be determined from the table of t-values with $N(s) - M(s)$ degrees of freedom [$N(s)$ is the number of equations] and Equation 39. The confidence limits will be given by $\pm t_a S[q_1(s)]$, where a is the probability of a value of t greater than t_a.

Now the possible systematic error in the answer must be determined. First, estimate the maximum moment of the source by using Equation 45. Then, determine the value of $Q^s(\mathbf{k})$ appropriate to the particular probe configuration used, the sample volume, and the order of fit for the sth axis. This can be done by the rather tedious procedure presented in the last section. Once this is done, the error can be estimated from Equations 47a or 47b.

Obviously, the procedure described would be very tedious if done by hand. However, on a computer the task is easily accomplished. Let us now turn to the task of evaluating the procedure.

*These can be taken to be the calibration accuracy of the probe.

CHAPTER V

EVALUATION

Quantitative Tests

Thus far, the theory has been developed qualitatively. The equations and procedures have been developed without consideration of any experimental limitations that may be present. Also, the fundamental assumption upon which the method is based has been justified by a more or less intuitive argument. There is no way to determine how often this assumption can be expected to hold true. Therefore, it is necessary that some procedure be devised to test this method in order to determine its feasibility as a technique for determination of the dipole moment of a spacecraft.

The simplest way to do this is to use the near-field method to determine the magnetic moments of sources whose actual moments are already known. If the sources selected for analysis are numerous and varied, general conclusions can be drawn as to the validity of this technique. Specifically, the testing program is aimed at answering these questions: Can one expect to determine a reasonably accurate value for the dipole moment of an object by this procedure, and is the uncertainty in this number small enough to be useful?

In view of the complexity of the calculations involved in such an analysis, the test program was carried out entirely on a computer. That is, a program was written which would generate magnetic data for a given set of arbitrarily located point dipoles and then analyze these data by the method presented above (see Appendix B). In this way, a large number of different cases could be analyzed in a short time. These cases would also be free from any experimental error which could be confused with the systematic errors associated with the technique itself. To determine the sensitivity of the technique to the experimental errors, provisions were also made in the program to introduce errors into the data which would simulate errors encountered in an actual test.

A modified version of this program was used to determine the error functions $E_j(\mathbf{k})$ on spheres of different radii. Hence, the systematic errors could be estimated for each test case by the foregoing procedure.

Test Procedure

In these tests, it was assumed that the maximum number of magnetometers available would be four. The major parameters of interest in a test were the ratio of the source diameter to the radius to the closest sensor, and the order of fit of the near-field equations. The parameters varied from test to test were the radii of the various probes and the configurations of these probes.

The tests were conducted in three sections. The first section was concerned with the determination of the moment of a single point dipole located somewhere within a sphere of known diameter. These tests were fairly extensive and the results used to compute the error functions $E_j(k)$ for a given probe configuration, order of fit, and sphere diameter. Also, the order of magnitude of each of the lower order multipole coefficients in the near-field expansion could be estimated from these results. This is helpful in attempts to estimate the magnitudes of the coefficients of an aggregate of dipoles. The results were also helpful in determining the effects of machine error in the computations and the behavior of the least squares coefficients as a function of the order of fit.

The second section of the tests was concerned with multiple magnet sources. Naturally, these tests could not be as extensive as the ones above, because of the many possibilities in the construction of the sources. Sources containing up to 28 dipoles were analyzed. For a given probe configuration, the moments, and their variances, of each of the sources were determined as a function of the order of fit.

In the third section, the same sources as in the second section were analyzed. In this case, however, the data were adjusted to simulate real data, and the effect on the calculations was studied.

In an experimental environment, there will be a minimum observable change in the magnetic field because of the limitations of the instrumentation. This threshold value will not be constant but will be dependent upon the values of the magnetic field seen on the sensors.* Real data will therefore be subject to a minimum uncertainty. Also, the magnetometers have a certain calibration accuracy that must be taken into consideration. Errors in the data within these limits were also introduced.

Obviously, all possible errors could not be simulated. The reason for these tests was to determine whether or not errors of the type described previously are detectable from observations of the calculated values of the multipole moments and whether or not limits could be placed on these moments when this type of error was present.

Each source was tested using from one to four probes in both the zero and the +1 configuration. This procedure permitted each of the various probe configurations to be evaluated.

*The magnitude of the fields observed will determine the range setting of the magnetometers. The higher the range, the greater the threshold value will be.

CHAPTER VI

RESULTS

Accuracy

The tests show that this method of analysis is indeed effective. They also allow general predictions to be made about its capabilities in a given situation. Of primary interest is the accuracy of this technique.

The accuracy of this technique (defined here as the ability to predict the correct values for the dipole-moment coefficients) is a function of several variables. These variables can be divided into two classes: (I) Variables associated with the magnetic source itself and over which one has no control (e.g., strength and location of the magnetic components); and (II) variables associated with the technique (e.g., number and location of the probes and the order of fit to the near-field equations). The variation in accuracy produced by the Class I variables is the most significant and, unfortunately, the most difficult to deal with. That produced by the Class II variables is for the most part predictable and is usually much smaller than the variation due to Class I parameters. Therefore let us consider Class II first.

The Class II variables can in turn be divided into two subclasses: (1) physical variables such as the number of probes and the configuration of these probes, and (2) the order of fit. There appears to be a complicated interrelationship between the accuracy and the physical variables. Studies of the error functions $E_j(k)$ for each probe arrangement possible with from one to four probes and for several different sets of probe radii show that there is a definite change in accuracy if one of the parameters is changed; however, this change is usually small. The numbers $Q^1(k)$ and $Q^3(k)$ are a measure of the maximum possible error in the measurement of a magnet located on the surface of a sphere of radius k (see Figure 2). The characteristics of different probe configurations are shown in Table 1; corresponding values of Q^1 and Q^3 are shown in Tables 2 and 3 for different size parameters S_p (defined as the source diameter divided by the radius to the closest probe) and order of fit.

These results permit one to compare the various probe configurations. In general, a given number of probes in the +1 configuration are more accurate than the same number of probes in the zero configuration (for a certain sample size and order of fit). In addition, the probes provide more information* about the magnetic field of the source, and this information permits calculations to be carried out to higher order.

*That is, the number of equations for a given axis is larger than for the zero configuration.

Table 1—Selected probe configurations.

Configuration	Type	Number of Probes	Probe Radii ($r_{1j} = r_1/r_j$)			
			r_{11}	r_{12}	r_{13}	r_{14}
1	+1	4	1	2/3	1/2	2/5
2	+1	4	1	1/2	1/3	1/4
3	+1	4	1	5/6	5/7	5/8
4	+1	3	1	2/3	1/2	
5	+1	3	1	1/2	1/3	
6	+1	2	1	2/3		
7	0	4	1	2/3	1	1
8	0	4	1	1/2	1	1
9	0	4	1	2/3	1/2	1/2
10	0	3	1	1	1	

For probes in the +1 configuration, it appears that the accuracy decreases somewhat as the probe spacing decreases. However, this effect is important only for very close spacing, and in general the variation of accuracy is unpredictable. This means that one can assume that the probe spacing is not critical.

The order of magnitude of the change in accuracy as a function of the order of fit is also observable in Tables 2 and 3. This change is obviously more drastic than the other changes and is definitely predictable. The tables show that as the order of fit is increased, the accuracy improves. The apparent discrepancy observable in the higher orders of fit is believed due to machine errors in the computations. This point will be discussed more fully later.

The same behavior was observed when multiple dipole sources were tested.* That is, the absolute accuracy remained about the same for all probe configurations tested with a particular sample and a given order of fit and got increasingly better as the order of fit was increased. Again, the discrepancy in accuracy was noted as the order of fit became fairly high, and as before, it was assumed to be due to machine error.

The variation as a function of the size parameter S_p is also easy to characterize. As the size of the sample is increased, the accuracy decreases. This is due to the increase in the magnitude of the multipole moment coefficients as the magnetic material is displaced further from the center of the object. This type of variation is really tied in with the Class I variables, which are considered later.

The accuracy as a function of the source parameters is much more difficult to analyze. This accuracy is dependent on the values of the various multipole moment coefficients of the

*The data used in these analyses were considered "perfect".

Table 2–Values of Q^1 for selected probe configurations.

Size Parameter S_p	Configuration	Order of Fit						
		1	2	3	4	5	6	7
0.4	1	0.13901	0.0039488	0.00003915	0.00001025	0.00000349	0.00000995	0.00000837
	2	0.12232	0.0039475	0.00006992	0.00000291	0.00000259	0.00000574	0.00000175
	3	0.12824	0.0045939	0.00009143	0.00001109	0.00000595	0.00004668	0.00056881
	4	0.13944	0.0040254	0.00003694	0.00001092	0.00000445		
	5	0.14551	0.0037651	0.00007186	0.00000317	0.00000402		
	6	0.14089	0.00419	0.00001967				
	7	0.081034	0.018571	0.00039829	0.00000672			
	8	0.087116	0.019120	0.00036852	0.00000837			
	9	0.13830	0.0015225	0.00011698	0.00000350			
	10	0.088199	0.019279					
0.6	1	0.29908	0.01812	0.00040640	0.00003516	0.00000569	0.0000173	0.00001552
	2	0.26348	0.018058	0.00071926	0.00001203	0.00000423	0.00000950	0.00000270
	3	0.27632	0.020997	0.00092398	0.00003790	0.00001026	0.00009265	0.0011069
	4	0.29999	0.018466	0.00038315	0.00003621	0.00000737		
	5	0.31291	0.017250	0.00073907	0.00001258	0.00000662		
	6	0.3031	0.0192	0.00020491				
	7	0.24835	0.097130	0.0045043	0.00003703			
	8	0.26437	0.099920	0.0041643	0.00018160			
	9	0.29747	0.0067129	0.0012293	0.00001845			
	10	0.26738	0.10074					
0.8	1	0.52035	0.054118	0.0020232	0.00030860	0.00001208	0.00002730	0.00002628
	2	0.45609	0.054393	0.0037083	0.00010345	0.00000640	0.00001412	0.00000369
	3	0.47795	0.063327	0.0048125	0.00033310	0.00002863	0.00017379	0.0020098
	4	0.52196	0.055190	0.0019150	0.00031762	0.00001466		
	5	0.54547	0.051762	0.0038109	0.00010783	0.00000988		
	6	0.52750	0.057537	0.0010723				
	7	0.63746	0.32796	0.025616	0.00039433			
	8	0.67300	0.33698	0.023657	0.0017447			

Table 2 (continued)–Values of Q^1 for selected probe configurations.

Size Parameter S_p	Configuration	Order of Fit						
		1	2	3	4	5	6	7
0.8	9	0.51801	0.022397	0.0063067	0.00016617			
	10	0.68006	0.33967					
1.0	1	0.85543	0.14429	0.0079381	0.0021425	0.00009264	0.00004305	0.0004290
	2	0.74244	0.14615	0.015732	0.00068123	0.00001328	0.00002001	0.00000468
	3	0.77575	0.17022	0.020620	0.0023200	0.00027406	0.00035247	0.0036208
	4	0.85814	0.14723	0.0073447	0.00220801	0.00009856		
	5	0.89990	0.13863	0.016169	0.00071035	0.00001591		
	6	0.8676	0.15383	0.00373				
	7	1.5286	0.91619	0.10295	0.002561			
	8	1.6045	0.94099	0.094992	0.010326			
	9	0.85274	0.06508	0.023189	0.00088478			
	10	1.6203	0.94833					
1.2	1	1.4622	0.37326	0.027578	0.013383	0.00080394	0.00009329	0.00007073
	2	1.2464	0.38442	0.062195	0.0039409	0.00007129	0.00002966	0.00000570
	3	1.2959	0.44705	0.082707	0.014533	0.0025463	0.0011433	0.0062675
	4	1.4670	0.38128	0.024838	0.013825	0.00084557		
	5	1.5474	0.36242	0.063934	0.0041143	0.00005070		
	6	1.4842	0.40011	0.010361				
	7	3.7073	2.4203	0.34892	0.012653			
	8	3.8748	2.4811	0.32174	0.046700			
	9	1.4608	0.18972	0.079101	0.0039053			
	10	3.9110	2.4999					
1.4	1	2.7402	1.03678	0.093961	0.085541	0.0075137	0.00099240	0.00022100
	2	2.2770	1.0917	0.25550	0.022826	0.0054193	0.00006971	0.00000866
	3	2.3508	1.26175	0.33878	0.092237	0.025252	0.068796	0.11577
	4	2.7500	1.0603	0.08050	0.08859	0.0078824		
	5	2.9211	1.0220	0.26269	0.02386	0.00033284		
	6	2.7839	1.1182	0.031555				

Table 2 (concluded)–Values of Q^1 for selected probe configurations.

Size Parameter S_p	Configuration	Order of Fit						
		1	2	3	4	5	6	7
1.4	7	10.033	6.8975	1.1750	0.056014			
	8	10.456	7.0636	1.0833	0.20573			
	9	2.7448	0.58509	0.27260	0.015633			
	10	10.5509	7.1163					

Table 3–Values of Q^3 for selected probe configurations.

Size Parameter S_p	Configuration	Order of Fit			Size Parameter S_p	Configuration	Order of Fit		
		1	2	3			1	2	3
0.4	1	0.1566	0.0051880	0.00008308	1.0	1	0.83068	0.14346	0.012987
	2	0.16362	0.0030402	0.00002303		2	0.87703	0.081955	0.0039768
	3	0.14484	0.0072891	0.00025152		3	0.74015	0.21665	0.046100
	4	0.1573	0.0054296			4	0.83341	0.15065	
	5	0.16386	0.0032509			5	0.87833	0.087407	
	6	0.15876				6	0.84315		
	7	0.21510	0.018625			7	2.6890	0.91858	
	8	0.21749	0.01904			8	2.7140	0.93646	
	9	0.13605	0.0034622			9	0.73895	0.11821	
	10	0.21795				10	2.7192		
0.6	1	0.32077	0.023574	0.00084925	1.2	1	1.5463	0.40008	0.051806
	2	0.33434	0.014003	0.00024306		2	1.6400	0.21115	0.012235
	3	0.29842	0.032721	0.0024838		3	1.3518	0.62490	0.20518
	4	0.56441	0.097380			4	1.5515	0.42064	
	5	0.33481	0.14964			5	1.6425	0.22673	
	6	0.32494				6	1.5704		
	7	0.56441	0.099480			7	6.0039	2.4179	
	8	0.57038	0.024655			8	6.0565	2.4623	
	9	0.27673	0.016863			9	1.3848	0.23419	
	10	0.57154				10	6.0676		
0.8	1	0.50401	0.064527	0.0040985	1.4	1	3.0718	1.1283	0.20238
	2	0.52386	0.039034	0.0012096		2	3.2770	0.57289	0.044889
	3	0.47259	0.088139	0.011496		3	2.6112	1.8461	0.89865
	4	0.50548	0.67424			4	3.0825	1.1886	
	5	0.52457	0.041678			5	3.2820	0.61591	
	6	0.51036				6	3.1219		
	7	1.2568	0.32968			7	15.396	6.8312	
	8	1.2693	0.33647			8	15.525	6.9503	
	9	0.43033	0.05086			9	2.7694	0.41841	
	10	1.2718				10	15.553		

source under observation; hence, it varies greatly from source to source. As mentioned above, when the size of the source is increased, the error usually increases; however, when sources of the same size are examined, predictions about the absolute accuracy of the results are in general difficult to make. In fact, unless one has more information about the source than its physical size, absolute predictions are impossible. That is, it is impossible to say, for a given set of physical parameters, order of fit, and source dimensions, that the dipole moment of any source can be calculated to within so many magnetic moment units. This is because the magnitude of the error is dependent upon the strengths of the magnetic components of the source: The more "magnetic" the source, the larger the error will be.

The tests do show, however, a limit (in magnetic moment units) on the magnitude of the error for sources of a particular size and magnetization as a function of the order of fit.

Table 4 shows the maximum errors observed as a function of the order of fit and sample size for 54 samples containing from 9 to 28 magnetic components (most of which were located at the outer edge of the source). These numbers were obtained with the probes in configuration number 1 (see Table 1). Since the horizontal and vertical moment calculations are inherently dissimilar, separate entries are made for each. The value of the actual dipole moment, M, is shown to the right of the observed error θ.

This table is not meant to give any general accuracy predictions. However, the magnitudes of the magnetic components in the sources are much larger than are usually found in a spacecraft; hence, the errors in this table are expected to be larger than those actually seen. If some other source were tested, larger errors could very conceivably be obtained.

Let us now turn to the question of whether or not one can estimate the accuracy of a given calculation: first, for ideal data (i.e., data for a perfect system) and second, for real data that is subject to errors of some type.

Effect and Estimation of Errors

In the tests described above, errors in the calculations are either machine errors or systematic errors. As one can see from Tables 2 and 3, machine error becomes apparent only at the higher orders of fit; this error is due to the rounding off of the numbers calculated by the computer. This effect is also illustrated in Table 5, which table presents the variation of the calculated multipole fields* for a centered dipole as the order of fit is varied (again for probes in configuration number 1). Note that even at its worst, this effect is very small in the dipole moment and can usually be neglected.

The systematic errors obviously are not negligible; however, they can be estimated by the procedure described in the text. This was done for each of the sources tested. Table 6 compares the calculated systematic error limits with the observed errors shown in Table 4. These numbers are representative of the results in general in that in every case tested, the observed error was less than the limits calculated by the estimate of $|e_1(s)|$ given by

*These numbers are the multipole coefficients ($a_{2j-1,1}$) divided by the smallest radius raised to the $2j + 1$ power and hence are in the magnetic field units (nanotesla).

Table 4—Largest errors observed in dipole-moment calculations (values in 10^{-3} A-m^2).

Size Parameter S_p		Order of Fit													
		1		2		3		4		5		6		7	
		θ	M	θ	M	θ	M	θ	M	θ	M	θ	M	θ	M
0.4	H	222.3	2512	3.6	144	0		0		0		0		0	
	V	189.0	972	3.5	640	0		—		—		—		—	
0.6	H	477.1	2512	18.3	1604	0		0		0		0		0	
	V	444.0	972	15.7	640	0		—		—		—		—	
0.8	H	+795.1	2512	58.0	1604	2.1	1850	0		0		0		0	
	V	822.0	972	41.1	640	3.5	640	—		—		—		—	
1.0	H	1146.2	2512	148.0	1604	6.9	1850	2.1	1604	0		0		0	
	V	1308.0	972	111.0	275	17.4	972	—		—		—		—	
1.2	H	1499.0	2512	353.0	1604	18.1	1500	11.7	1604	0		0		0	
	V	1825.0	972	287.0	275	57.3	972	—		—		—		—	
1.4	H	1855.0	1500	881.0	1604	57.0	1172	67.8	1604	5.0	1604	0		0	
	V	2388.0	275	761.0	275	155.0	572	—		—		—		—	

Note: θ = observed error.
H = error in horizontal dipole-moment component.
V = error in vertical dipole-moment component.
M = true value of dipole-moment component.
0 = errors less than 10^{-3} A-m^2.

Table 5—Calculated x-axis multipole coefficients for a centered dipole for probe configuration 1 (values in nanoteslas).

Coefficient	Order of Fit						
	1	2	3	4	5	6	7
a_1	80.0	80.0	79.999999618	80.000004821	80.000039196	79.993561739	79.987034380
a_3		0.0	−0.000000507	0.000019175	0.000158821	−0.054924022	−0.154667296
a_5			−0.000000202	0.000024517	0.000295795	−0.197767705	−0.905817656
a_7				0.000009742	0.000252243	−0.338142809	−2.742426869
a_9					0.00079690	−0.269945145	−4.308601377
a_{11}						−0.081082108	−3.295361917
a_{13}							−0.967441047

Table 6—Comparison of the observed errors with the estimated systematic error limits (values in 10^{-3} A-m^2).

Size Parameter S_p		Order of Fit													
		1		2		3		4		5		6		7	
		θ	E	θ	E	θ	E	θ	E	θ	E	θ	E	θ	E
0.4	H	222	522	3.6	11.8	0	0	0	0	0	0	0	0	0	0
	V	189	531	3.5	22.5	0	0								
0.6	H	477	1137	18.3	43.70	0	1.8	0	0	0	0	0	0	0	0
	V	444	1149	15.7	103	0	3.7								
0.8	H	795	2005	58.0	136	2.1	6.6	0	1.3	0	0	0	0	0	0
	V	822	1918	41.1	288	3.5	18.3								
1.0	H	1146	3352	148	381	6.9	27.2	2.1	5.7	0	0	0	0	0	0
	V	1308	3359	111	266	17.4	52.5								
1.2	H	1499	5821	353	1046	18.1	131	11.7	37.5	0	3.8	0		0	0
	V	1825	6638	287	854	57.3	222								
1.4	H	1855	13730	881	3144	57.0	378	67.8	259	5.0	22.8	0	2.8	0	0
	V	2388	7636	761	2805	155	818								

Note: θ = observed error.
E = estimated error limit.
0 = errors less than 10^{-3} A-m^2.

$$|e_1(1)| = |e_1(2)| = Q^1(\mathbf{k})B_e \tag{47a}$$

and

$$|e_1(3)| = Q^3(\mathbf{k})B_e \ . \tag{47b}$$

Note that for the lower orders of fit, the estimated errors are quite large. This indicates that in order to obtain meaningful results, a given calculation must be made with order 2 or greater. The minimum order of fit is dependent on the value of Q^1 or Q^3 for a given sample size and probe configuration. Values of Q^1 or Q^3 of the order of 0.01 or less will give acceptable limits. Using these criteria, the minimum orders of fit can be determined for the probe configurations given in Tables 2 and 3.

The results of these tests indicated that the technique is indeed a useful method of dipole-moment determination if the data used are almost perfect. In an actual test situation, however, this is not the case. Real data will be subject to a much larger roundoff error than computer-generated data. This error is due to instrumentation limitations and is dependent on the magnitudes of the magnetic field observed at a particular probe location. For testing purposes, it was assumed that the minimum observable value of magnetic field is $0.1S$ nanotesla, where S is a scale factor determined by the maximum value of magnetic field H_m seen at a particular radius. For a particular value of H_m, the scale factor S used in the tests can be determined from Table 7.

The data used in each of the foregoing tests were modified by being rounded off to the nearest $0.1S$ nanotesla; then they were reanalyzed. As was expected, changes in the resultant calculations were observed, but they were in general small when compared with the systematic error already present. Table 8 shows the changes observed for the x-axis dipole-moment component for one particular source ($S_p = 1.4$) measured with probes in configuration number 1.

Table 8 shows the important effects of the roundoff process. Notice first of all that the values calculated from the truncated data are in general more accurate than the values using perfect data. This effect was observed most often in the first and second orders of fit. It is indirectly due to the

Table 7—Determination of scale factor S.

Range of H_m (nanoteslas)		S
From	To	
0	100	1
100	200	2
200	500	5
500	1000	10
1000	2000	20
2000	5000	50
5000	10,000	100

Table 8—Dipole-moment calculations for a $0.7r_1$-diameter source (actual dipole moment was 1.500 A-m^2.).

Order of Fit	Perfect Data (10^{-3} A-m^2)		Rounded Data (10^{-3} A-m^2)		Systematic Tolerance (10^{-3} A-m^2)
	Moment	Statistical Tolerance	Moment	Statistical Tolerance	
1	3355.11		1897.47		13730.0
2	1221.46		1467.84		5194.3
3	1555.70		1536.53		470.70
4	1470.62	6.30	1496.34	1.43	428.50
5	1502.74	1.06	1500.80	1.13	37.60
6	1499.88	0.03	1499.48	0.27	4.97
7	1499.99	0.01	1497.97	2.63	1.11

accuracy assigned to the rounded magnetic field values. The uncertainty due to roundoff at each of the data points is $\pm 0.05S$, where S is the scale factor for that particular probe location. This uncertainty varies from location to location (since the field levels vary). This means that the weights w_i of each of the near-field equations will be different for each probe location. Since field levels are higher on the closer probes, the equations for these probes will be weighted less than those for the farther probes. This means that the systematic errors which arise from the closer probes (which are in general larger than those from the farther probes) will be correspondingly reduced. In the cases where perfect data were used, all the equations were weighted equally, allowing the total systematic error to be larger.

Another effect of the roundoff is a slightly increased error as the order of fit is increased. This is noticeable in the table for orders of fit 6 and 7. This effect is believed to be due in part to roundoff of the data and in part to machine error.

Up to this point, the statistical uncertainty in the calculations has been neglected. This was because the uncertainty in the perfect data was very small, and the uncertainty in the calculation was mostly due to systematic errors. However, when real data are used, the corresponding uncertainty in the calculations becomes important. As the order of fit is increased, the systematic uncertainty decreases. In general, this is accompanied by an increase in the statistical uncertainty. In assigning limits to the answer, one must choose the larger of the two. This was done for each case tested and it was found that the actual error was within the limits predicted unless the order of fit was fairly high (see Table 8).

Note that the uncertainty due to machine error has not been taken into account. The statistical uncertainty is due to roundoff of the data, whereas machine errors are due to roundoff of any number calculated by the computer. However, as was stated before, the machine errors are important only if the order of fit is high.

CHAPTER VII

DETECTION OF ERRORS

In an actual test situation, the accuracy usually assigned to the data is not the threshold accuracy of the instrumentation but the calibration accuracy (which is in general much larger). Errors in the data within these limits are to be expected, and their effect on the accuracy of the technique must be examined. In order to do this, the data used in the previous tests were modified to simulate linear calibration errors and were then reanalyzed. The results show that these errors are indeed significant and that their effect increases with the order of fit. However, comparison of the results shows that these errors can be detected from observations of the behavior of the higher order multipole coefficients as a function of the order of fit.

The calibration accuracy assigned to a given data point was, as before, dependent on the maximum field level seen at that particular probe location. This accuracy was assumed to be $\pm S$ nanotesla,* where S is the same scale factor as before. The data points were modified by errors of the form $D' = aD$, where D is the actual data point, D' is the new data point, and a is the error factor ($0.99 \leqslant a \leqslant 1.01$) for a particular probe location and sensor.

In order to be able to detect the presence of errors, one must know what type of behavior to expect of the calculated multipole coefficients as the order of fit is changed. A few tests were run on single- and double-dipole sources whose multipole coefficients were easily calculable (from Equations 40 and 41). Two observations were made from these tests.

The first was that the actual multipole coefficients of each of the sources decreased significantly as the index of the coefficient was increased, even though the size of the source was large ($S_p = 1.4$). In the worst cases, the coefficients decreased by about a factor of 2 as the index was raised by 1. Table 9 compares the actual x-axis multipole coefficients** (for an x-axis dipole displaced from the center of the source by a distance of $0.6r_1$ along the $+x$ axis) with those calculated by near-field analysis.

The second observation was that the changes in the coefficients became smaller and smaller as the order of fit increased. These coefficients also steadily approached the true values (until machine error became significant).

*This corresponds to an accuracy of 1 percent of the maximum field level observable on that particular range.

**Henceforth, whenever "multipole coefficients" are mentioned, it will refer to the actual multipole coefficients (given by Equations 16a and b) divided by r_1^{j+1} and expressed in nanotesla.

Table 9–Multipole coefficients for a single displaced dipole, where $a_j = a_{j1}/r_1^{j+2}$ and Δa_j is the change in the coefficient as one goes from one order of fit to the next.

Coefficient	Actual Value (nanoteslas)	Calculated Value (nanoteslas)						
		Order of Fit						
		1	2	3	4	5	6	7
a_1	80.00	188.58	51.69	82.03	78.95	80.06	80.00	79.98
Δa_1		136.89	30.34	3.08	1.11	.06	.02	
a_3	−21.6		−53.80	−12.60	−25.60	−21.08	−21.66	−21.82
Δa_3			41.2	13.0	4.52	.58	.16	
a_5	+6.48			16.61	−0.35	8.26	6.17	5.06
Δa_5				16.96	8.61	2.09	1.11	
a_7	−2.04				−6.80	.72	−2.87	−6.47
Δa_7					7.52	3.59	3.6	
a_9	+0.661					2.43	−0.44	−6.34
Δa_9						2.87	5.90	
a_{11}	−0.218						−0.87	−5.49
Δa_{11}							4.62	
a_{13}	+0.0730							−1.38

These results suggest the behavior one can expect for an arbitrary source. Since the multipole coefficients of a source are in fact combinations of the coefficients for single off-centered dipoles, and since the latter coefficients decrease rapidly as the index becomes large, the coefficients of a composite source can be expected to exhibit the same general behavior. That is, the higher order coefficients will in general be much smaller than those at the lower end of the multipole spectrum of the source. Also, these higher order coefficients will in general decrease rapidly as the index is increased. It might be argued that by careful selection of the locations and magnitudes of the dipoles within the source, a particular multipole coefficient can be set to any desired magnitude in relation to the other coefficients. This is indeed true; however, the number of parameters that must be specified increases rapidly with the index. This means that the probability of a coefficient at the high end of the spectrum (i.e., above the fifth coefficient) having a relatively high value will be small if the dipoles are randomly placed within the source. The same thing cannot be said of the lower coefficients. Hence, one can expect large variations from source to source at the low end of the spectrum.

The behavior of the calculated coefficients for an arbitrary source is not at all predictable. However, in general, large changes can be expected in these coefficients until the order of fit is at least equal to the number of the most significant coefficients of the source. After this, the changes in the coefficients should be small (until machine error becomes important). If the real coefficients of the source decrease as the index increases throughout the multipole spectrum, the changes in the calculated coefficients can be expected to decrease as the order of fit is increased.

The results of many tests on sources whose multipole coefficients were not known in detail seem to bear this theory out. Table 10 shows the calculated x-axis coefficients for a source ($S_p = 1.2$) containing 20 dipoles. Notice the decrease in the magnitude of these coefficients as the index increases. Notice also that the magnitudes of the changes in the coefficients in general decrease as the order of fit is increased* (up to order of fit 6). These results are typical of each case tested.

When errors were introduced into the data, either by rounding off the data points or by introducing calibration factors, this behavior was changed. The effect of the errors was the same as that caused by machine error with the exception that it occurred at a lower order of fit. It was characterized by increasingly large changes in the calculated multipole coefficients as the order of fit was increased. The magnitudes of the calculated coefficients also became very large. When the data used in the previous analyses was rounded off and reanalyzed, the results shown in Table 11 were obtained.

Table 12 gives the results of the analysis of the same data containing calibration errors. Notice that the dipole moment values are affected the least by the presence of this error. Table 13 compares the observed error in the dipole moment with the predicted error limits (either statistical or systematic, whichever is larger) for the above cases. Note that in each case, machine error becomes significant in the higher orders of fit. Again, these results are typical in that the error limits are in general predictable unless the machine error is large. The presence of this error is characterized by large fluctuations in the calculated values of the multipole coefficient from one order of fit to the next and by unrealistic values for the higher order multipole coefficients (specifically, for Table 12, order of fit 7).

*The large changes in the dipole and octopole moments from order of fit 2 to 3 are probably due to a fairly large moment ($a_5 = 130$ nanotesla).

Table 10–Multipole coefficients (in nanoteslas) for a $1.2r_1$-diameter source calculated using perfect data. True dipole coefficient = 115.44 nanoteslas, and Δa_j is the change in the coefficient from one order of fit to the next.

Coefficient	Order of Fit						
	1	2	3	4	5	6	7
a_1	−20.59	67.50	−109.25	−116.28	−115.26	−115.42	−115.45
Δa_1		88.09	176.75	7.03	1.02	0.16	0.03
a_3		34.62	−205.41	−235.14	−230.95	−232.36	−232.68
Δa_3			240.03	29.73	4.19	1.41	0.32
a_5			96.80	−135.60	−127.62	−132.69	−134.51
Δa_5				38.8	7.98	5.07	1.82
a_7				−15.56	−8.58	−17.27	−22.59
Δa_7					6.98	8.69	5.32
a_9					+2.25	−4.68	−12.86
Δa_9						6.93	8.18
a_{11}						−2.08	−8.25
Δa_{11}							6.17
a_{13}							−1.79

Table 11–Multipole coefficients (in nanoteslas) for a $1.2r_1$-diameter source calculated using rounded data. True dipole coefficient = 115.44 nanoteslas, and Δa_j is the change in the coefficient from one order of fit to the next.

Coefficient	Order of Fit						
	1	2	3	4	5	6	7
a_1	−2.88	10.67	−108.16	−115.57	−115.63	−115.40	−115.87
Δa_1		13.55	118.83	7.41	.06	.23	.47
a_3		10.40	−207.69	−233.18	−233.52	−231.72	−237.91
Δa_3			218.09	25.49	.07	1.8	6.19
a_5			−98.24	−133.62	−134.52	−128.10	−164.90
Δa_5				35.38	.9	6.42	36.8
a_7				−14.89	−15.89	−4.77	−116.51
Δa_7					1.00	11.12	11.74
a_9					−0.38	8.66	−166.91
Δa_9						9.04	175.57
a_{11}						+2.77	−131.45
Δa_{11}							134.22
a_{13}							39.38

Table 12–Multipole coefficients for a $1.2r_1$-diameter source calculated using "uncalibrated" data. True dipole coefficient = 115.44 nanoteslas, and Δa_j is the change in the coefficient from one order of fit to the next.

Coefficient	Order of Fit						
	1	2	3	4	5	6	7
a_1	−3.03	10.69	108.23	−115.93	−116.29	−117.08	−122.49
Δa_1		13.72	118.92	7.70	.36	.79	5.4
a_3		10.52	−207.85	−234.10	−236.12	−242.33	−313.11
Δa_3			218.37	26.25	2.02	6.21	70.78
a_5			−98.37	−134.81	−140.01	−162.21	−583.13
Δa_5				36.44	5.2	22.20	420.92
a_7				−15.33	−21.12	−59.54	−1337.49
Δa_7					5.79	38.42	1277.95
a_9					−2.19	−33.46	−2041.48
Δa_9						31.27	2008.02
a_{11}						−9.57	−1544.59
Δa_{11}							1545.02
a_{13}							−450.36

Table 13—Observed errors and computed error limits for dipole moments in Tables 10, 11, and 12 (values in nanoteslas).

Order Of Fit	Perfect Data (Table 10)		Rounded Data (Table 11)		Uncalibrated Data (Table 12)	
	Observed Error in a_1	Calculated Limits	Observed Error in a_1	Calculated Limits	Observed Error in a_1	Calculated Limits
1	−118.56	4187	−112.56	4187	−140.52	4187
2	−228.68	1069	−126.11	1069	−13.36	1069
3	−7.74	78.96	−7.28	78.96	−8.92	78.96
4	+1.06	38.32	+0.13	38.32	+0.61	38.32
5	−0.23	2.30	+0.19	2.30	+1.07	2.30
6	−0.02	0.27	−0.04	0.27	+2.06	1.18*
7	−0.01	0.20	+0.43	0.78*	+8.81	4.56*

*Statistical error limit (other values indicate estimated systematic errors).

To recapitulate, the errors associated with this near-field technique vary with the order of fit to the near-field equations. They can be divided into three groups: systematic errors, data errors, and machine errors. The first of these, the systematic errors, predominate at low orders of fit (M = 1, 2, and 3) and decrease rapidly as the order of fit is increased. The data errors (i.e., those caused by imperfect data) are present at every order of fit but tend to become larger as the order of fit is increased.

These two types of errors are similar in that limits can be placed upon them (which were valid in every case tested). Machine errors, on the other hand, are caused by roundoff of numbers by the computer and are very hard to estimate. Fortunately, they are noticeable only at high orders of fit (usually M = 6 or 7), and their presence can be detected by careful observation of the results.

CHAPTER VIII

CONCLUSIONS

This paper has presented a detailed description of a new technique that can be used to determine the magnetic dipole moment of a spacecraft or any other magnetic source. The major advantage of the technique is that the data required are always easily obtained and easily analyzed (on a computer).

An extensive testing program was conducted to verify the theory. In all, over 2000 analyses were performed, over 500 of which were on composite sources. The results of the tests allow several conclusions to be drawn about the technique.

First, the best results are obtained if all the sensors are located along the x axis (i.e., in the +1 configuration). The spacing of the probes is not really critical, but care should be taken to ensure that they are neither too close together ($r_{max}/r_{min} \leqslant 2$) nor too far apart ($r_{max}/r_{min} \geqslant 4$).

Second, the magnitude of the errors obtained will decrease as r_1 (the smallest probe radius) is increased. However, accurate answers were obtained for sources whose diameters were $1.4r_1$. If possible, r_1 should be approximately the diameter of the smallest sphere enclosing the source.

Third, the intermediate orders of fit (M = 3, 4, 5) will, in general, give the answers with the smallest uncertainty. For orders of fit lower than this, the systematic uncertainty will, in general, be too large to be useful. For orders of fit larger than this, the possibility of large machine errors exists. However, higher orders of fit can be used, provided that the changes in the higher coefficients are taken into account. Analyses in which the coefficients exhibit large fluctuations or unrealistic values should be suspect.

It should be noted that the z-axis calculations are different from those of the x and y axes in that one has much less data to work with. Although the calculations for this axis are just as valid as for the x and y axes, they should not be expected to be as accurate. Also, in an actual test situation, care should be taken to ensure that there is no zero level uncertainty on the z-axis sensors of the probes before data are taken, because this will also introduce large errors.

In estimating the systematic errors for a given test case, one can use the values of Q^1 and Q^3 presented in Tables 2 and 3. To do this, choose the probe configuration and size parameter S_p that best fit the particular test situation. This will provide only an approximate value for Q^1 and Q^3. However, since the actual errors were much smaller than the estimated errors for the lower orders of fit, these values are not critical.

The test cases used to verify this technique were fairly extensive; but it is not assumed that they covered all possibilities. However, the sources used were considerably more magnetic than the average spacecraft.* Hence, one can assume that the errors obtained were larger (in magnetic moment units) than would actually be observed.

At any rate, the technique was found to work well in every case tested. It is believed that it will work well in any case in which one can obtain good data. It is also not unreasonable to assume that further study will yield a completely computerized version of this technique.

*That is, their magnetic components were stronger.

ACKNOWLEDGMENTS

It is a pleasure to thank Mr. William Mocarsky and Mr. Anthony Villasenor for their assistance in developing the computer programs necessary for the evaluation and implementation of this technique.

Goddard Space Flight Center
National Aeronautics and Space Administration
Greenbelt, Maryland, April 22, 1971
186-68-50-01-51

REFERENCES

1. Eichhorn, W. L., "A New Method for Determining the Magnetic Dipole Moment of a Spacecraft From Near-Field Data", NASA Technical Memorandum X-63765, August 1969.

2. Boyle, J. C., et al., "A Theoretical Approach to the Determination of Magnetic Torques by Near-Field Measurement", NASA Technical Note D-4485, May 1968.

3. Lackey, M. H. "The Reaction of a Rigid Body to a Uniform Force Field", NOL T269-60, Naval Ordnance Laboratory, Washington, D.C.

4. Edmonds, A. R., *Angular Momentum in Quantum Mechanics,* Princeton: Princeton University Press, 1960.

BIBLIOGRAPHY

Blatt, J. M., and Weisskopf, V. F., *Theoretical Nuclear Physics,* New York: John Wiley and Sons, 1952.

Della Torre, E., and Longo, C. U., *The Electromagnetic Field,* Boston: Allyn and Bacon, Inc., 1969.

Goulden, C. H., *Methods of Statistical Analysis,* New York: John Wiley and Sons, Inc., 1952.

Guest, P. G., *Numerical Methods of Curve Fitting,* New York: Cambridge University Press, 1961.

Hobson, E. W., *The Theory of Spherical and Ellipsoidal Harmonics,* New York: Chelsea Publishing Co., 1955.

Jackson, J. D., *Classical Electrodynamics,* New York: John Wiley and Sons, 1963.

MacMillan, W. D., *The Theory of the Potential,* New York: Dover Publications, Inc., 1958.

McQuistan, R. B., *Scalar and Vector Fields,* New York: John Wiley and Sons, Inc., 1965.

Smythe,W. R., *Static and Dynamic Electricity,* New York: McGraw-Hill Book Co., Inc., 1950.

Stratton, J. A., *Electromagnetic Theory,* New York: McGraw-Hill Book Co., Inc., 1941.

Weatherburn, C. E., *Advanced Vector Analysis,* G. Bell and Sons, Ltd., 1947.

Appendix A

Vector Spherical Harmonics

Vector spherical harmonics arise when a vector field is transformed by a rotation of its frame of reference. This type of transformation is more complicated than that of a scalar field because the components of the vector field are dependent upon the axes of the particular frame of reference.

The rotation of a frame can be described in terms of an "operator" $\mathbf{J} = \mathbf{L} + \mathbf{S}$, where $\mathbf{L}$ is the angular momentum operator $-i\mathbf{r} \times \nabla$ and $\mathbf{S}$ is the spin operator, whose components are

$$\mathbf{S}_1 = i\mathbf{u}_1 \times \ , \mathbf{S}_2 = i\mathbf{u}_2 \times \text{, and } \mathbf{S}_3 = i\mathbf{u}_3 \times \ .$$

The operators $\mathbf{L}$ and $\mathbf{S}$ each have their own sets of eigenfunctions. For the operator $\mathbf{L}$, the spherical harmonics Y_{jm} satisfy the relations

$$L^2 Y_{jm} = j(j+1)Y_{jm}$$

and

$$L_z Y_{jm} = mY_{jm} \ .$$

For the spin operator $\mathbf{S}$, the vectors $\mathbf{e}_q$ are defined by

$$\mathbf{e}_{+1} = -\frac{1}{\sqrt{2}}(\mathbf{u}_1 + i\mathbf{u}_2) \ ,$$

$$\mathbf{e}_0 = \mathbf{u}_3 \ ,$$

and

$$\mathbf{e}_{-1} = \frac{1}{\sqrt{2}}(\mathbf{u}_1 - i\mathbf{u}_2) \ ,$$

such that

$$S^2 \mathbf{e}_q = 2\mathbf{e}_q$$

and

$$S_z \mathbf{e}_q = q\mathbf{e}_q \ .$$

It is convenient to construct eigenfunctions of the operator $\mathbf{J}$ similar to those above for $\mathbf{L}$ and $\mathbf{S}$. Since the operators $\mathbf{L}$ and $\mathbf{S}$ commute with each other, and each satisfies the commutation relations

$$(L_1, L_2) = iL_3 \ , (L_2, L_3) = iL_1 \ , (L_3, L_1) = iL_2$$

and

$$(S_1, S_2) = iS_3 \ , \text{ etc.},$$

this is easily done by means of the vector addition law. This law states that if $\mathbf{J}_1$ and $\mathbf{J}_2$ are two angular momentum operators which satisfy the above commutation rules and which commute with each other, and if $Y_{im}(q)$ is the angular momentum eigenfunction of the operator $\mathbf{J}_q$ such that

$$J_q^2 y_{jm}(q) = j(j+1)y_{jm}(q)$$

and

$$J_{qz} y_{im}(q) = m y_{jm}(q) ,$$

eigenfunctions of the operator $J = J_1 + J_2$ can be constructed from products of the functions $y_{jm}(1)y_{qr}(2)$. This product is an eigenfunction of the operator $\mathbf{J}_z = \mathbf{J}_{1z} + \mathbf{J}_{2z}$ with eigenvalue $M = m + r$, but is not an eigenfunction of the operator $\mathbf{J}^2 = \mathbf{J}_x^2 + \mathbf{J}_y^2 + \mathbf{J}_z^2$. However, linear combinations of the products $y_{jm}(1)y_{qr}(2)$ can be used to form simultaneous eigenfunctions of the operator $\mathbf{J}^2$ and $\mathbf{J}_z$. This eigenfunction will be denoted by G^M_{Jjq} and will be defined by

$$G^M_{Jjq} = \sum_{m=-j}^{+j} \sum_{r=-q}^{+q} C_{jq}(J, M; m, r) y_{jm}(1) y_{jm}(2) , \tag{A-1}$$

where the quantities C_{jq} are real numbers known as Clebsch-Gordan coefficients. These coefficients exhibit the properties that

$$C_{jq} = 0 \quad \text{unless} \quad M = m + r ,$$

and

$$J = j + q,\ j + q - 1,\ \ldots,\ |j - q| .$$

The functions G^M_{Jjq} are eigenfunctions of the operator J^2 with eigenvalue $J(J+1)$ and of the operator J_z with eigenvalue M.

Now, eigenfunctions of the operator $\mathbf{J} = \mathbf{L} + \mathbf{S}$ may be constructed using the functions $\mathbf{e}_q$ and Y_{jm}. (These eigenfunctions are the vector spherical harmonics $\mathbf{Y}^M_{Jj1}$ defined as $\mathbf{Y}^M_{Jj}$ in the text.*) They are given by

$$\mathbf{Y}^M_{Jj1} = \sum_{m=-j}^{+j} \sum_{q=-1}^{+1} C_{j1}(J, M; m, q) Y_{jm}(\theta, \phi) \mathbf{e}_q . \tag{A-2}$$

The values of C_{j1} can be computed from Table A-1 (taken from Reference 4).

One is now interested in how the vector spherical harmonics behave when operated on by the various vector operators (e.g., $\nabla \cdot$; $\nabla \times$). The following equations were obtained from Reference 4, and some will be stated without proof. In these equations, the function f is a scalar function of the radial coordinate only.

*The third subscript is equal to 1 because $S^2\mathbf{e}_q = 2\mathbf{e}_q = S(S+1)\mathbf{e}_q$; hence, Y^M_{Jjs} becomes Y^M_{Jj1}.

Table A-1—Clebsch-Gordan coefficients $C_{j1}(J, M; j, q)$.

	$q = 1$	$q = 0$	$q = -1$
$J = j + 1$	$\left[\frac{(j+M)(j+M+1)}{2j+1)(2j+2)}\right]^{1/2}$	$\left[\frac{(j-M+1)(j+M+1)}{(2j+1)(j+1)}\right]^{1/2}$	$\left[\frac{(j-M)(j-M+1)}{(2j+1)(2j+2)}\right]^{1/2}$
$J = j$	$-\left[\frac{(j+M)(j-M+1)}{(2j)(j+1)}\right]^{1/2}$	$\left[\frac{M^2}{j(j+1)}\right]^{1/2}$	$\left[\frac{(j-M)(j+M+1)}{(2j)(j+1)}\right]^{1/2}$
$J = j - 1$	$\left[\frac{(j-M)(j-M+1)}{(2j)(2j+1)}\right]^{1/2}$	$-\left[\frac{(j-M)(j+M)}{j(2j+1)}\right]^{1/2}$	$\left[\frac{(j+M)(j+M+1)}{(2j)(2j+1)}\right]^{1/2}$

$$\nabla \times (f\mathbf{Y}^M_{j,j+1}) = i\left(\frac{d}{dr} + \frac{j+2}{r}\right) f\left(\frac{j}{2j+1}\right)^{1/2} \mathbf{Y}^M_{jj} \ , \tag{A-3}$$

$$\nabla \times (f\mathbf{Y}^M_{j,j-1}) = i\left(\frac{d}{dr} - \frac{j-1}{r}\right) f\left(\frac{j+1}{2j+1}\right)^{1/2} \mathbf{Y}^M_{jj} \ , \tag{A-4}$$

$$\nabla \times (f\mathbf{Y}^M_{jj}) = i\left(\frac{d}{dr} - \frac{j}{r}\right) f\left(\frac{j}{2j+1}\right)^{1/2} \mathbf{Y}^M_{j,j+1} + i\left(\frac{d}{dr} + \frac{j+1}{r}\right) f\left(\frac{j+1}{2j+1}\right)^{1/2} \mathbf{Y}^M_{j,j-1} \ , \tag{A-5}$$

$$\nabla \cdot (f\mathbf{Y}^M_{j,j+1}) = -\left(\frac{j+1}{2j+1}\right)^{1/2} \left(\frac{d}{dr} + \frac{j+2}{r}\right) f Y_{jM} \ , \tag{A-6}$$

$$\nabla \cdot (f\mathbf{Y}^M_{j,j-1}) = \left(\frac{j}{2j+1}\right)^{1/2} \left(\frac{d}{dr} - \frac{j}{r}\right) f Y_{jM} \ , \tag{A-7}$$

$$\nabla \cdot (f\mathbf{Y}^M_{jj}) = 0 \qquad \text{(for any } f\text{)} \ , \tag{A-8}$$

$$\mathbf{L}Y_{jm} = -i\mathbf{r} \times \nabla Y_{jm} = \sqrt{j(j+1)}\, \mathbf{Y}^M_{jj} \ , \tag{A-9}$$

and

$$\nabla(fY_{jm}) = -\left(\frac{j+1}{2j+1}\right)^{1/2} \left(\frac{d}{dr} - \frac{j}{r}\right) f\mathbf{Y}^m_{j,j+1} + \left(\frac{j}{2j+1}\right)^{1/2} \left(\frac{d}{dr} + \frac{j+1}{r}\right) f\mathbf{Y}^M_{j,j-1} \ . \tag{A-10}$$

The above equations can be proven in the following manner. First of all, the expression for the quantity $\nabla_q f(r) Y_{jm}$ is needed, where ∇_q is the qth spherical component of ∇. This can be shown to be equal to (Reference 4, p. 80)

$$\left(\frac{j+1}{2j+3}\right)^{1/2} C_{j1}(j+1, m+q; m, q)\left(\frac{\partial}{\partial r} - \frac{j}{r}\right) fY_{j+1,m+q}$$

$$- \left(\frac{j}{2j-1}\right)^{1/2} C_{j1}(j-1, m+q; m, q)\left(\frac{\partial}{\partial r} + \frac{j+1}{r}\right) fY_{j-1,m+q} \cdot \qquad \text{(A-11)}$$

Consider now the quantity

$$\nabla \cdot (f\mathbf{Y}_{Jj}^{M}) \cdot$$

This is equal to

$$\sum_{m=-j}^{+j} \sum_{q=-1}^{+1} \sum_{r=-1}^{+1} \mathbf{e}_r^* \cdot \mathbf{e}_q \; \nabla_r Y_{jm} C_{j1}(J, M; m, q)$$

$$= \sum_{m=-j}^{+j} \sum_{q=-1}^{+1} \nabla_q Y_{jm} C_{j1}(J, M; m, q)$$

$$= \left(\frac{j+1}{2j+3}\right)^{1/2} \left(\frac{\partial}{\partial r} - \frac{j}{r}\right) f \sum_{m=-j}^{+j} \sum_{q=-1}^{+1} C_{j1}(J, M; m, q) C_{j1}(j+1, m+q; m, q) Y_{j+1,m+q}$$

$$- \left(\frac{j}{2j-1}\right)^{1/2} \left(\frac{\partial}{\partial r} + \frac{j+1}{r}\right) f \sum_{m=-j}^{j} \sum_{q=-1}^{+1} C_{j1}(J, M; m, q) C_{j1}(j-1, m+q; m, q) Y_{j-1,m+q} \cdot$$

However, because $m + q = M$, the quantities $Y_{j\pm1,m+q}$ are independent of the summation over m and q. Hence, since Clebsch-Gordan coefficients have the property that

$$\sum_{m=-j}^{+j} \sum_{m'=-j'}^{+j'} C_{jj'}(J, M; m, m') C_{jj'}(J', M'; m, m') = \delta_{JJ'} \delta_{MM'} ,$$

this expression can be reduced to

$$\nabla \cdot (f\mathbf{Y}_{Jj}^{M}) = \left(\frac{j+1}{2j+3}\right)^{1/2} \left(\frac{\partial}{\partial r} - \frac{j}{r}\right) fY_{j+1,M} \delta_{J-1,j} - \left(\frac{j}{2j-1}\right)^{1/2} \left(\frac{\partial}{\partial r} + \frac{j+1}{r}\right) fY_{j-1,M} \delta_{J+1,j} \cdot$$

Substitution of the values $J + 1$, $J - 1$, and J for j yields Equations A-6, A-7, and A-8, respectively. The proofs of the other equations are similar.

Appendix B

Near-Field Computer Program

A listing of the program used to generate data for the near field of a system of dipoles and also used in the near-field analysis of these data is presented in this appendix.

Let us define B_r, B_θ, and B_ϕ as the components with respect to an origin 0 of the magnetic field **B** of a point dipole (moment = **m**) located at the point **k** (see Figure B-1). The equations for B_r, B_θ, and B_ϕ are as follows:

$$B_r(r, \theta, \phi) = \frac{3\mathbf{m} \cdot (\mathbf{r} - \mathbf{k})}{\omega^{5/2}} \psi_1 - \frac{\mathbf{m} \cdot \mathbf{r}}{\omega^{3/2}} ,$$

$$B_\theta(r, \theta, \phi) = - \frac{3\mathbf{m} \cdot (\mathbf{r} - \mathbf{k})}{\omega^{5/2}} \psi_2 - \frac{\mathbf{m} \cdot \theta}{\omega^{3/2}} ,$$

and

$$B_\phi(r, \theta, \phi) = \frac{3\mathbf{m} \cdot (\mathbf{r} - \mathbf{k})}{\omega^{5/2}} \psi_3 - \frac{\mathbf{m} \cdot \phi}{\omega^{3/2}} ,$$

where

$$\psi_1 = k(\sin\theta \sin\theta_m \cos(\phi - \phi_m) + \cos\theta \cos\theta_m) ,$$

$$\psi_2 = k(\cos\theta \sin\theta_m \cos(\phi - \phi_m) - \sin\theta \cos\theta_m) ,$$

$$\psi_3 = k(\sin\theta_m \sin(\phi - \phi_m) ,$$

and

$$\omega = r^2 + k^2 - 2r\psi_1 .$$

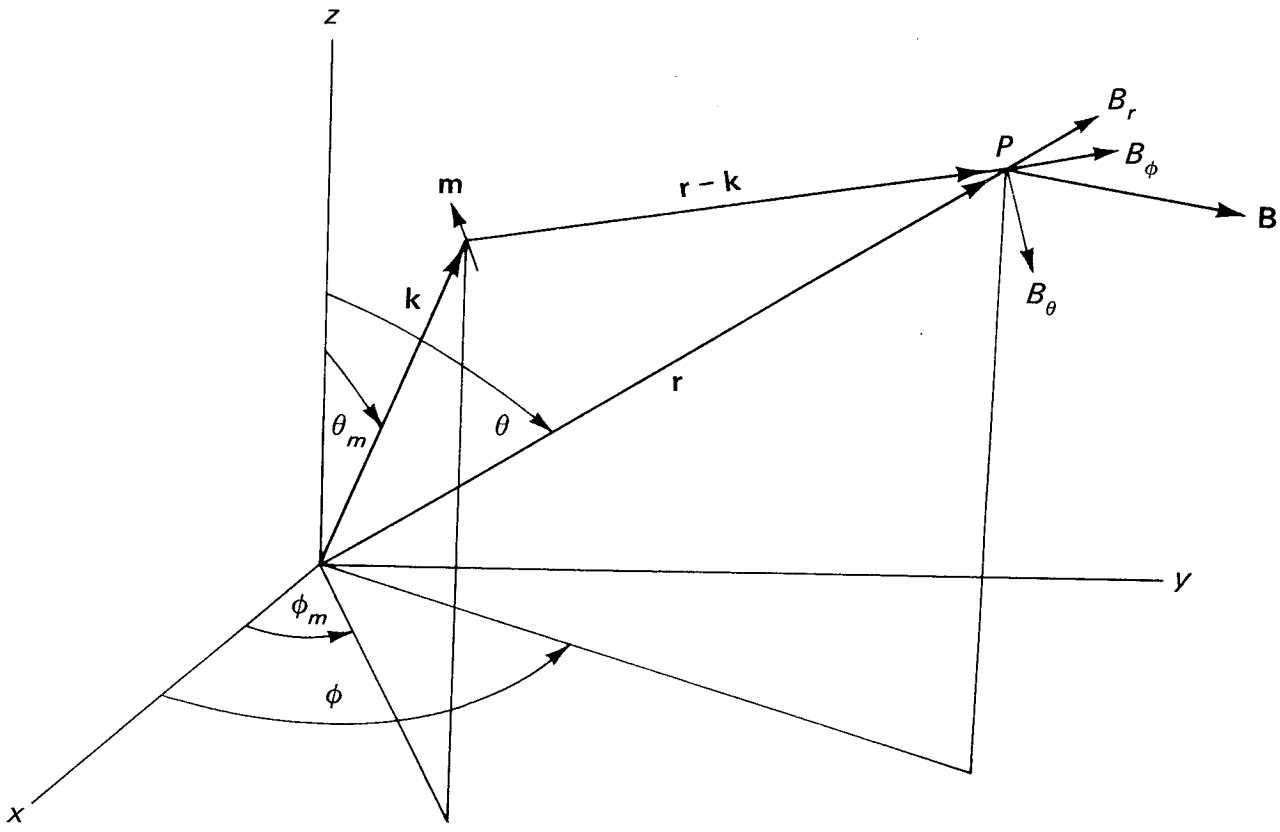

Figure B-1—The magnetic field **B** of a dipole **m** at the point *P*.

```
      PROGRAM NRFIELD
C     TO GENERATE NEAR FIELD MAGNETIC DATA
      EQUIVALENCE (ALPHA(1),HX(1)),(BETA(1),HX(26)),(GAMMA(1),HX(51))
      EQUIVALENCE (DA(1),HY(1)),(DB(1),HY(26)),(DC(1),HY(51))
      DIMENSION MX(100), MY(100), MZ(100),D(100), TD(100), PD(100)
      DIMENSION DVX(4),DVY(4),DVZ(4)
      DIMENSION R(4), THETA(4), COEF(20)
      DIMENSION CX(4), SX(4), CY(4), SY(4),DCZ(4)
      DIMENSION CXD(4),SXD(4), CYD(4), SYD(4), DCZD(4)
      DIMENSION QX(8), QY(8),QZ(8), QXD(8), QYD(8),QZD(8)
      DIMENSION ITITLE(20)
      DIMENSION HX(36,4 ), HY(36,4 ), HZ(36,4 )
      DIMENSION X(36),Y(36), Z(36), PHI(36),PH(36)
      DIMENSION T(10)
      DIMENSION ALPHA(25),BETA(25),GAMMA(25),DA(25),DB(25),DC(25)
      REAL MUPX,MUPY,MUPZ,MUR,MUT,LR,LT,LP ,MUP
      REAL MX,MY,MZ,MLY,MLZ,MLX,ML,MURX,MURY,MURZ,MUTX,MUTY,MUTZ
      REAL MAX,MIN
C
C     ZERO OUT ARRAYS
      DO 450 I = 1,4
       CX(I) = CY(I) = SX(I) = SY(I) = DCZ(I) = 0.
      CXD(I) = SXD(I) = CYD(I) = SYD(I) = DCZD(I) = 1.
      ALPHA(I) = BETA(I) = GAMMA(I) = 0.
      DVX(I) = DVY(I) = DVZ(I) = 1.
      DA(I) = DB(I) = DC(I) = 0.
      II = I + 4
      QX(I) = QY(I) = QZ(I) = 0.
       QX(II) = QY(II) = QZ(II) = 0.
      QXD(II) = QYD(II) = QZD(II) = 1.
      QXD(I) = QYD(I) = QZD(I) = 1.
      HX(I) = HY(I)= HZ(I)= 0.
  450 CONTINUE
      T(1) = 6.314
      T(3)=2.353
      T(2)=2.920
      T(4)=2.132
      T(5)=2.015
      T(6)=1.943
      T(7)=1.895
      T(8)=1.860
      T(9)=1.833
      T(10)=1.812
    3 FORMAT(6F10.0)
    1 FORMAT(8F10.0)
    2 FORMAT(10I5)
 1111 READ(60,2) NUM,ICON,NORDER
      IF(NUM) 430,430,350
  350 READ(60,1)( R(I),I = 1,NUM)
  428 READ(60,2) ND
      IF(ND) 1111,1111,429
  429 READ(60,3)(MX(I),MY(I),MZ(I),D(I),TD(I),PD(I), I = 1,ND)
      JO = 0
      DO 4061 I = 1,ND
      IF(R(1)-D(I)) 4062,4062,4061
 4062 WRITE(61,4063) I
```

```
 4063 FORMAT( 20X, 12HERROR IN D(    ,13,2H)    ,/)
      JQ = 1
 4061 CONTINUE
      IF(JQ) 4065,4065,428
 4065 CONTINUE
      DO 300 I = 1,NUM
  300 THETA(I) = 90.
      IF(ICON) 301,301,302
  301 THETA(NUM) = 180.
      THETA(NUM - 1) = 0.
  302 CONTINUE
    5 DO 10 I=1,NUM
   10 THETA(I)=THETA(I)*.01745327
      DO 625 I=1,ND
      TD(I) = TD(I)*.01745327
      PD(I) = PD(I)*.01745327
  625 CONTINUE
      NTERMS = NTERM2 = 1
      NP = NUM
      LQ = 0
      JJ = 0
      DO 521 L = 1,36
  521 PH(L) = FLOAT(L - 1 )*10.
      DO 90 J=1,NUM
      PHI=-.1745327
      DO 601 L = 1,36
  601 X(L) = Y(L) = Z(L) = 0.
      LQ = 1
      DO 100 K=1,36
      PHI=PHI+.1745327
      PHIK=PHI
      HR=HT=HP=0.
      RJ=R(J)
      SINTJ=SIN(THETA(J))
      COSTJ=COS(THETA(J))
      DO 80 I=1,ND
C     CALCULATE MAGNETIC FIELD AT RJ,THETA(J),PHI(K) DUE TO POLE I
      CS=SINTJ*SIN(TD(I))*COS(PHIK-PD(I))
      ALPH =CS+COSTJ*COS(TD(I))
      BET =COSTJ*SIN(TD(I))*COS(PHIK-PD(I))-SINTJ*COS(TD(I))
      GAMM =SIN(TD(I))*SIN(PHIK-PD(I))
      Q=RJ*RJ+D(I)*D(I)-2.*RJ*D(I)*ALPH
      CS=RJ*SINTJ*COS(PHIK)-SIN(TD(I))*COS(PD(I))*D(I)
      MLX=MX(I)*CS
      MLY=MY(I)*(RJ*SINTJ*SIN(PHIK) -D(I)*SIN(TD(I))*SIN(PD(I)))
      MLZ=MZ(I)*(RJ*COSTJ-D(I)*COS(TD(I)))
      ML=MLX+MLY+MLZ
      CS=3.*ML/(SQRT(Q)*Q*Q)
      MURX=MX(I)*SINTJ*COS(PHIK)
      MURY=MY(I)*SINTJ*SIN(PHIK)
      MURZ=MZ(I)*COSTJ
      MUTX=MX(I)*COSTJ*COS(PHIK)
      MUTY=MY(I)*COSTJ*SIN(PHIK)
      MUTZ=-MZ(I)*SINTJ
      MUPX=-MX(I)*SIN(PHIK)
      MUPY=MY(I)*COS(PHIK)
```

```
      MUPZ=0.
      MUR=MURX+MURY+MURZ
      MUT=MUTX+MUTY+MUTZ
      MUP=MUPX+MUPY+MUPZ
      Q1=1./(SQRT(Q)*Q)
      LR=MUR*Q1
      LT=MUT*Q1
      LP=MUP*Q1
C     MAGNETIC FIELDS
      BR=CS*(RJ-D(I)*ALPH )-LR
      BT=-CS*D(I)*BET -LT
      BP=CS*D(I)*GAMM -LP
C     TOTAL FIELD
      HR=HR+BR
      HT=HT+BT
      HP=HP+BP
   80 CONTINUE
      DIFF=THETA(J)-1.5708
      IF(DIFF) 20,30,40
   20 IF(ABS(DIFF)-.01) 30,30,25
   25 Z(K)   =-HR*100000.
      X(K)   =HT*100000.
      Y(K)   =-HP*100000.
      GO TO 360
   30 X(K)   =HR*100000.
      Z(K)   =HT*100000.
      Y(K)   =-HP*100000.
      GO TO 360
   40 IF(ABS(DIFF)-.01) 30,30,45
   45 Z(K)   =HR*100000.
      X(K)   =-HT*100000.
      Y(K)   =-HP*100000.
  360 CONTINUE
  101 FORMAT( 10X ,3(F20.10,2X),/)
  102 FORMAT( 10X, I5)
      HX(K,J) = X(K)
      HY(K,J) = Y(K)
      HZ(K,J) = Z(K)
  100 CONTINUE
C  HAVE MAGNETIC FIELD
C  NOW CALL FOURIER ANALYSIS SUBROUTINES
  372 FORMAT(/,20X,19HCOEF FOR PROBE NO.    ,I1)
C
C
      CALL FOURIER(NORDER, X,COEF)
      CX(J) = COEF(2)
      SX(J) = COEF(3)
      CALL FOURIER(NORDER, Y,COEF)
      SY(J) = COEF(3)
      CY(J) = COEF(2)
      CALL FOURIER(NORDER, Z,COEF)
      DC7(J) = COEF(1)
  380 CONTINUE
      IF(NP-J) 504,504,503
  503 IF(4-J) 504,504,90
  504 JJ = JJ+1
```

```
      NP = NP-4
      LQ = 0
      ISTART = (JJ-1)*J + 1
      ISTOP = JJ * 4
      WRITE(61,155)(I,I=ISTART,ISTOP)
  155 FORMAT (1H1,4(16X,5HPROBE,I2,10X),//,6H THETA,6X,1HX,9X,1HY,9X,1HZ
     1,3(12X,1HX,9X,1HY,9X,1HZ)/)
      DO 2245 K = 1,36
      WRITE(61,156) PH(K),(HX(K,L),HY(K,L),HZ(K,L),L = 1,4)
 2245 CONTINUE
  156 FORMAT(1X,F5.1,3(1X,F9.3),3(4X,F9.3,1X,F9.3,1X,F9.3))
      IF(ICON) 4020,4020,4030
 4020 NJ = NUM - 2
      GO TO 4031
 4030 NJ = NUM
 4031 CALL MAXMIN(MAX,MIN,36,HX(1,NJ))
      R3 = R(NJ)*R(NJ)*R(NJ)*.00001
      BX = .25*(MAX-MIN)*R3
      CALL MAXMIN(MAX,MIN,36,HY(1,NJ))
      BY = .5*(MAX-MIN)*R3
      CALL MAXMIN(MAX,MIN,36,HZ(1,NJ))
      B1 = ABS(MAX)
      B2 = ABS(MIN)
      IF(B1-B2)  4070,4070,4080
 4080 BZ = MAX*R3
      GO TO 4071
 4070 BZ = MIN*R3
 4071 CONTINUE
      B =  SQRT(BX*BX + BY*BY+BZ*BZ)
  501 DO 502 I = 1,4
      DO 502 L = 1,36
      HX(L,I) = HY(L,I) = HZ(L,I) = 0.
  502 CONTINUE
 2250 CONTINUE
C
   90 CONTINUE
C     AT THIS POINT ALL CALCULATIONS ARE COMPLETE
C     FROM HERE ON IS MAINLY OUTPUT- PLOTTING AND PRINTING
C
C     PRINT SECTION
C
C     CHANGE PHI FROM RADIANS TO DEGREES
      PHI(1)=0.
      DO 150 I=2,36
  150 PHI(I)=PHI(I-1)+10.
      IF(IZ.EQ.1) 1112,1113
 1112 WRITE(61,151)
  151 FORMAT(//////////,20X,45HMAGNETIC FIELD CALCULATIONS--PROBE LOCATI
     1ONS    )
      DO 161 I= 1,NUM
      THETA(I) = THETA(I)/ .01745327
  161 CONTINUE
      WRITE(61,152)(I,R(I),THETA(I),I=1,NUM)
  152 FORMAT(43X,6HPROBE(,I1,20H) IS LOCATED AT R = ,F11.4,13H CM. THETA
     1 = ,F11.4,1X,7HDEGREES    /)
 1113 WRITE(61,153) ND
```

```
  153 FORMAT(//,20X,18HFIELD PRODUCED BY ,I2,22H DIPOLES DETERMINED BY )
      DO 162 I = 1, ND
      TD(I) = TD(I)/.01745327
      PD(I) = PD(I)/.01745327
  162 CONTINUE
      WRITE(61,154)(I,MX(I),I,MY(I),I,MZ(I),I,D(I),I,TD(I),I,PD(I),I=1,
     1ND)
  154 FORMAT(1X,3HMX(,I2,2H)=,F11.4,1X,3HMY(,I2,2H)=,F11.4,1X,3HMZ(,I2,
     12H)=,F11.4,1X,2HD(,I2,2H)=F11.4,1X,3HTD(,I2,2H)=,F11.4,1X,3HPD(,I2
     2,2H)=,F11.4)
      DN=0.
      DE=0.
      DD=0.
      DO 1010 I=1,ND
      DN=DN+MX(I)
      DE=DE-MY(I)
 1010 DD=DD-MZ(I)
      WRITE(61,1011) DN,DE,DD
      WRITE(61,4032) B
 4032 FORMAT(20X,27HMAGNETIZATION ESTIMATION =    ,F20.10,//)
 1011 FORMAT(9(/),45X, 20HTOTAL DIPOLE MOMENTS  ,//,50X,7HNORTH =,
     1F11.4, / ,50X, 6HEAST = ,F11.4,/, 50X, 7HDOWN =    , F11.4,////)
C  PLACE F.C.'S IN PROPER FORM FOR MATRIX
      IF(ICON) 401,401,402
  401 N = NUM-2
      CXA3 =.25*(CX(NUM-1)+CX(NUM)+SY(NUM-1)+SY(NUM))
      SXA3 = .25*(SX(NUM-1)+SX(NUM)-CY(NUM-1)-CY(NUM))
      DCZA3 = .5*(DCZ(NUM-1)+DCZ(NUM))
      CXA3D = .5
      SXA3D = .5
      DCZA3D = .707
      GO TO 403
  402 N = NUM
  403 DO 404 I = 1,N
      NN = I+N
      QX(I) = CX(I)
      QX(NN) = -SY(I)
      QY(I) = SX(I)
      QY(NN) = CY(I)
      QZ(I) = DCZ(I)
  404 CONTINUE
      IF(ICON) 405,405,406
  405 NM = 2*(NUM-2)
      QX(NM+1) = -CXA3
      QXD(NM+1)=CXA3D
      QY(NM+1)=-SXA3
      QYD(NM+1)=SXA3D
      QZ(N+1)=-DCZA3
      QZD(N+1) = DCZA3D
      NEQX = NM+1
      NEQZ = NUM-1
      GO TO 807
  406 NEQX = 2*NUM
      NEQZ = NUM
C  NOW EVERYTHING IS IN THE CORRECT FORM FOR SOLN BY MATRIXX
  807 CONTINUE
```

```
      WRITE(61,407)
  407 FORMAT(20X,2HR  , 13X, 3HQX  , 12X, 3HQXD , 12X, 3HQY  , 12X,
     1 3HQYD , 12X , 3HQZ  , 12X, 3HQZD , //)
  911 FORMAT( 15X, 7(F15.7 ,1X),/)
  912 FORMAT( 15X, 5(F15.7 ,1X),/)
      WRITE(61,911)(R(I) , QX(I), QXD(I),QY(I),QYD(I),QZ(I),QZD(I),
     1 I =1,N)
      DO 913 I = 1,N
      I2 = I + N
      WRITE(61,912) R(I),QX(I2),QXD(I2),QY(I2),QYD(I2)
  913 CONTINUE
      IF(ICON)410,410,411
  410 KL = 2*NUM -3
      WRITE(61,911)(R(N+1),QX(KL),QXD(KL),QY(KL),QYD(KL),QZ(N+1),
     1 QZD(N+1))
  411 CONTINUE
  426 CALL MATRIX(ICON,1,NUM,NEQX,NTERMS,R, QX,QXD,ALPHA,DA)
  420 CALL MATRIX(ICON,1,NUM,NEQX,NTERMS,R,QY,QYD,BETA,DB)
  803 FORMAT( 50X, 6HXAXIS  , /)
  804 FORMAT( 50X, 6HYAXIS  ,/)
  805 FORMAT( 50X, 6HZAXIS  , //)
      CALL MATRIX(ICON,0,NUM,NEQZ,NTERM2,R,QZ,QZD,GAMMA,DC)
      WRITE(61,27)
      DO 50 I = 1,NTERMS
      J = 2*I - 1
      WRITE(61,21)(J,ALPHA(I),DA(I),J,BETA(I),DB(I),J,GAMMA(I),DC(I))
   21 FORMAT (4H  A(,I2,6H,1) = ,F18.9,1X,2H+-,F10.5,
     1         4H  B(,I2,6H,1) = ,F18.9,1X,2H+-,F10.5,
     1         4H  A(,I2,6H,0) = ,F18.9,1X,2H+-,F10.5)
   50 CONTINUE
   27 FORMAT(30X, 32HCALCULATED MULTIPOLE COEFICIENTS  , //, 7X,
     1  6HX AXIS, 8X,8HVARIANCE, 8X, 6HY AXIS,8X, 8HVARIANCE,8X,
     1   6HZ AXIS, 8X, 8HVARIANCE,/)
C     CALCULATE MOMENTS
      RR=R(1)*R(1)*R(1)*.00001
      ALPHA(1)=ALPHA(1)*RR
      BETA(1)=-BETA(1)*RR
      GAMMA(1)=-GAMMA(1)*RR
      IR=NEQX-NTERMS
      DA(1) = DA(1)*RR*T(IR)
      DB(1)=DB(1)*RR*T(IR)
      IR=NEQZ-NTERM2
      DC(1)=DC(1)*RR*T(IR)
      WRITE(61,2050)ALPHA(1),DA(1),BETA(1),DB(1),GAMMA(1),DC(1)
 2050 FORMAT(4(/),10X,25HCALCULATED DIPOLE MOMENTS  ,20X,29H90 PERCENT
     1 CONFIDANCE LIMITS  ,/,20X,9HMNORTH =  ,F20.10,20X,F20.10,/,20X,
     19HMEAST  =  ,F20.10,20X,F20.10,/,20X,9HMDOWN =  ,F20.10,20X,F20.
     110,////)
C CHECK FOR ANOTHER ANALYSIS
      NTERMS = NTERMS + 1
      NTERM2 = NTERM2 + 1
      IF(NEQZ - NTERM2) 3008,3008,3009
 3008 NTERM2 = 1
 3009 IF(NEQX - NTERMS) 3010,3010,411
 3010 NTERMS = 1
      GO TO 426
```

```
  430 CONTINUE
      STOP
      END


      SUBROUTINE MATRIX(NCON, NAXIS, NR, NEQ, IP, R, A, D, Y,VY)
C  TO FORN WEIGHTED MATRIX EQUATIONS
      DIMENSION R(1),A(1), D(1)
      DIMENSION C(25,25) , M(25,25)
      DIMENSION Y(25),VY(25),X(25),RAD(4)
      DIMENSION Q(25,25)
      REAL M
      DO 1 I = 1,25
      X(I) = Y(I) = VY(I) = 0.
      DO 1 J = 1,25
    1 C(I,J) = M(I,J) = 0.
      DO 2 I = 1,NR
    2 RAD(I) = R(1)/R(I)
      IF(NCON) 6,6,3
    3 IF (NAXIS) 5,5,4
    4 N = NEQ/2
      GO TO 9
    5 N = NEQ
      GO TO 9
    6 IF(NAXIS)8,8,7
    7 N = (NEQ-1)/2
      GO TO 9
    8 N = NEQ-1
    9 DO 17 I = 1,N
      DO 17 J = 1,IP
      RR = RAD(I)**(2*J+1)
      F = 1.
      DF = 1.
      TJ = 1.
      DO 10 K = 1,J
      F = F*FLOAT(K)
      DF = DF*FLOAT(2*K-1)
   10 TJ = -2.*TJ
      FF = (-2.*FLOAT(J))/(TJ*F)
      RR = RR*FF*DF
      IF(NAXIS) 12,12,11
   11 C(I,J) = 2.*FLOAT(J)*RR
      IN = I + N
      C(IN,J) = RR
      GO TO 13
   12 C(I,J) = RR
   13 CONTINUE
      IF(NCON) 14,14,17
   14 RA = RAD(NR)**(2*J+1)
C COMPUTE C(NEQ,J) FOR D CONFIGURATION
      IF(NAXIS) 16,16,15
   15 C(NEQ,J) = FLOAT(2*J-1)*FLOAT(J)*RA
      GO TO 17
   16 C(NEQ,J) = 2. * FLOAT(J)*RA
   17 CONTINUE
```

```
C  HAVE (C(I,J) FO R      ALL CONFIGS AND AXES
C   CONSTRUCT LLSQ AND DATA MATRICES
      DO 18 J = 1,IP
      DO 18 I = 1,NEQ
   18 X(J) = X(J) +(A(I)*C(I,J))/(D(I)*D(I))
      DO 19 K = 1,IP
      DO 19 J = 1,IP
      DO 19 I =1,NEQ
   19 M(J,K) = M(J,K) + (C(I,J)*C(I,K))/(D(I)*D(I))
C HAVE WEIGHTED MATRICES
      DO 30 I = 1,IP
      Y(I) = X(I)
   30 CONTINUE
      CALL MATINV(M, IP, Y, 1, DETER)
C   Q IS NOW THE INVERSE OF M()( Y = MULTIPOLE MOMENTS
C COMPUTE DEVIATIONS AND RESIDUALS
      RES = 0.
      SS2 = 0.
      SR = 0.
      SQ = 0.
      DO 21 I = 1,NEQ
      FL = 0.
      DO 22 J = 1,IP
      FL = FL + C(I,J)*Y(J)
   22 CONTINUE
      S = (A(I)-FL)/D(I)
      RES = RES + S*S
      SS = S/A(I)
      SS = SQRT(SS*SS)
      SR = SR + S
      SQ = SQ + SS
      SS2 = SS2 + SS*SS
   21 CONTINUE
      IDF = NEQ - IP
      S2 = RES/ FLOAT(IDF)
  414 FORMAT( 10X,6(E15.7,2X))
  458 FORMAT(50X, 12HDATA MATRIX    ,/)
  451 FORMAT(2X,/,50X,20HMEASUREMENT MATRIX    ,/)
  452 FORMAT( 2X,/,50X,8HINVERSE    , /)
  453 FORMAT( 10X,11H PARAMETERS  ,/)
  454 FORMAT( 10X, 21HDEGREES OF FREEDOM = , I5,/,
     1 10X, 16HSIGMA SQUARED =    , E20.10 , /, 10X, 8HDETM =     ,
     1 E20.10 , /)
  412 FORMAT(10X,/,50X,20HNEAR FIELD MATRIX       ,//)
C  VARIANCE OF Y(I) = VY(I)
      DO 23 I = 1,IP
      QU = M(I,I)*S2
      IF(QU.LT.0.) 501,502
  501 WRITE(61,503)I,I,I,M(I,I),RES,NEQ,IP,S2
  503 FORMAT(10X,4HDEV( ,I2,1X,32H) IS NEGATIVE. PARAMETERS ARE.. ,/,
     110X,8HINVERSE(  ,I2,1H, ,I2,4H) =  ,F20.10,/, 10X,5HRES =  ,F20.14
     1,/,5HNEQ =   ,I2,2X,5HIP =   ,I2,2X,5HS2 =   ,F20.14)
      QU = -QU
  502 VY(I) = SQRT(QU)
   23 CONTINUE
      RETURN
      END
```

```
      SUBROUTINE MATINV(A,N,B,M,DETERM)
      DIMENSION IPIVOT(25),A(25,25),B(25,1),INDEX(25,2)
C                                                                      F
C     INITIALIZATION                                                   F
C                                                                      F
      DETERM=1.0
      DO 20 J=1,N                                                      F
   20 IPIVOT(J)=0                                                      F
      DO 550 I=1,N                                                     F
C                                                                      F
C     SEARCH FOR PIVOT ELEMENT                                         F
C                                                                      F
      AMAX=0.0                                                         F
      DO 105 J=1,N
      IF (IPIVOT(J)) 105,60
   60 DO 100 K=1,N                                                     F
      IF (IPIVOT(K)-1) 80, 100, 740
   80 IF(ABSF(A(J,K)).GT.ABSF(AMAX) ) 85,100
   85 IROW=J                                                           F
      ICOLUM=K
      AMAX=A(J,K)
  100 CONTINUE                                                         F
  105 CONTINUE
      IPIVOT(ICOLUM)=IPIVOT(ICOLUM)+1                                  F
C                                                                      F
C     INTERCHANGE ROWS TO PUT PIVOT ELEMENT ON DIAGONAL                F
C                                                                      F
      IF (IROW.EQ.ICOLUM) 260,140
  140 DETERM=-DETERM                                                   F
      DO 200 L  = 1, N
      SWAP=A(IROW,L)
      A(IROW,L)=A(ICOLUM,L)
  200 A(ICOLUM,L)=SWAP                                                 F
      IF(M) 210,260
  210 DO 250 L=1, M                                                    F
      SWAP=B(IROW,L)                                                   F
      B(IROW,L)=B(ICOLUM,L)                                            F
  250 B(ICOLUM,L)=SWAP                                                 F
  260 INDEX(I,1)=IROW                                                  F
      INDEX(I,2)=ICOLUM                                                F
      PIVOT =A(ICOLUM,ICOLUM)
      DETERM=DETERM*PIVOT
      PIVIN= 1.0/PIVOT
C     DIVIDE PIVOT ROW BY PIVOT ELEMENT                                F
C                                                                      F
      A(ICOLUM,ICOLUM)=1.0
      DO 350 L=1,N                                                     F
  350 A(ICOLUM,L)=A(ICOLUM,L)*PIVIN
      IF(M) 360,380
  360 DO 370 L=1,M                                                     F
  370 B(ICOLUM,L)=B(ICOLUM,L)*PIVIN
C                                                                      F
C     REDUCE NON-PIVOT ROWS                                            F
C                                                                      F
  380 DO 550 L1=1,N                                                    F
      IF(L1 .EQ.ICOLUM) 550,400
```

```
  400 T=A(L1,ICOLUM)                                                    F
      A(L1,ICOLUM)=0.0                                                  F
      DO 450 L=1,N                                                      F
  450 A(L1,L)=A(L1,L)-A(ICOLUM,L)*T                                     F
      IF(M) 460,550                                                     F
  460 DO 500 L=1,M                                                      F
  500 B(L1,L)=B(L1,L)-B(ICOLUM,L)*T                                     F
  550 CONTINUE                                                          F
C                                                                       F
C     INTERCHANGE COLUMNS                                               F
C                                                                       F
      DO 710 I=1,N                                                      F
      L=N+1-I
      IF (INDEX(L,1).EQ.INDEX(L,2) ) 710,630
  630 JROW=INDEX(L,1)                                                   F
      JCOLUM=INDEX(L,2)
      DO 705 K=1,N                                                      F
      SWAP=A(K,JROW)                                                    F
      A(K,JROW)=A(K,JCOLUM)
      A(K,JCOLUM)=SWAP
  705 CONTINUE                                                          F
  710 CONTINUE                                                          F
  740 RETURN                                                            F
      END
```

```
      SUBROUTINE FOURIER(NFIT,DATA,COEF)
C
C     CALCULATE FOURIER COEF UP TO AMPLITUDES OF SIN(NFIT*THETA)
C              AND COS(NFIT*THETA)
C     COEF(1)=DC TERM
C     COEF(2K) IS COEF OF COS(K*THETA)
C     COEF(2K+1) IS COEF OF SIN(K*THETA)
C
      DIMENSION DATA (1),COEF(1)
      A=0.
      DO 5 I=1,36
    5 A=A+DATA(I)
      COEF(1)=A/36.
      DO 100 N=1,NFIT
      THETA=-.1745327
      B1=T1=B2=T2=0.
      DO 50 J=1,36
      THETA=THETA+.1745327
      C=COS(N*THETA)
      S=SIN(N*THETA)
      B2=B2+S*S
      B1=B1+C*C
      T1=DATA(J)*C+T1
   50 T2=DATA(J)*S+T2
      ISTOR=2*N
      COEF(ISTOR)=T1/B1
  100 COEF(ISTOR+1)=T2/B2
      RETURN
      END
```

```
      SUBROUTINE LIST(AMP,NTERM,IFORMAT)
      DIMENSION AMP(1)
      GO TO(1,2,3) IFORMAT
    1 ID=1HX
      GO TO 4
    2 ID=1HY
      GO TO 4
    3 ID=1HZ
    4 J=2
      WRITE(61,300) ID,AMP(1)
  300 FORMAT(31X,2HDC,A1,3H = ,E11.4)
      DO 400 I=1,NTERM
      WRITE(61,100)I,ID,AMP(J),I,ID,AMP(J+1)
  100 FORMAT(30X,I2,1HC,A1,2H= ,E11.4,5X,I2,1HS,A1,2H= ,E11.4)
  400 J=J+2
      WRITE(61,500)
  500 FORMAT(/)
      RETURN
      END
```

```
      SUBROUTINE MAXMIN(AMAX,AMIN,N,PTS)
      DIMENSION PTS(1)
      AMAX=AMIN=PTS(1)
      DO 100 I=2,N
      AMAX=AMAX1(AMAX,PTS(I))
  100 AMIN=AMIN1(AMIN,PTS(I))
      RETURN
      END
```